From the first stars to the first black holes

Rosa Valiante,[1]★ Raffaella Schneider,[1] Marta Volonteri[2] and Kazuyuki Omukai[3]

[1]*INAF – Osservatorio Astronomico di Roma, via di Frascati 33, I-00040 Monteporzio Catone, Italy*
[2]*CNRS, UMR 7095, Institut d'Astrophysique de Paris, F-75014 Paris, France*
[3]*Astronomical Institute, Tohoku University, Aoba, Sendai 980-8578, Japan*

ABSTRACT

The growth of the first supermassive black holes (SMBHs) at $z > 6$ is still a major challenge for theoretical models. If it starts from black hole (BH) remnants of Population III stars (light seeds with mass ~ 100 $M_\odot$), it requires super-Eddington accretion. An alternative route is to start from heavy seeds formed by the direct collapse of gas on to an $\sim 10^5$ $M_\odot$ BH. Here we investigate the relative role of light and heavy seeds as BH progenitors of the first SMBHs. We use the cosmological, data constrained semi-analytic model GAMETE/QSODUST to simulate several independent merger histories of $z > 6$ quasars. Using physically motivated prescriptions to form light and heavy seeds in the progenitor galaxies, we find that the formation of a few heavy seeds (between 3 and 30 in our reference model) enables the Eddington-limited growth of SMBHs at $z > 6$. This conclusion depends sensitively on the interplay between chemical, radiative and mechanical feedback effects, which easily erase the conditions that allow the suppression of gas cooling in the low-metallicity gas ($Z < Z_{cr}$ and $J_{LW} > J_{cr}$). We find that heavy seeds cannot form if dust cooling triggers gas fragmentation above a critical dust-to-gas mass ratio ($\mathcal{D} \geq \mathcal{D}_{cr}$). In addition, the relative importance of light and heavy seeds depends on the adopted mass range for light seeds, as this dramatically affects the history of cold gas along the merger tree, by both SN- and AGN-driven winds.

Key words: black hole physics – galaxies: evolution – galaxies: high-redshift – galaxies: ISM – quasars: general.

1 INTRODUCTION

Supermassive black holes (SMBHs), powering the most luminous quasars ($>10^{47}$ erg s^{-1}) at redshift $z > 6$, are among the most intriguing and puzzling astronomical objects observed in the early Universe. Observational campaigns are pushing the high-redshift frontier closer and beyond the reionization epoch, expanding the census of high-redshift quasars.

The most distant quasar observed so far is ULAS J1120+0641, at $z \sim 7$, in which the central engine is a black hole (BH) with a mass of $M_{BH} = 2.0^{+1.5}_{-0.7} \times 10^9$ $M_\odot$ (Mortlock et al. 2011), already in place when the Universe was as old as ~ 700 Myr. Recently, Wu et al. (2015) discovered an ultraluminous quasar at $z \sim 6.3$ ($\sim 4 \times 10^{14}$ L$_\odot$) hosting a massive BH of $(1.2 \pm 0.19) \times 10^{10}$ $M_\odot$, presumably accreting close to the Eddington rate.

The existence of 10^9–10^{10} $M_\odot$ BHs in the early Universe (Fan et al. 2001, 2004; De Rosa et al. 2011, 2014, and references therein) poses a challenge to theoretical models aimed to explain the formation and growth of such massive objects. Many efforts have been done so far in order to unveil the nature of their progenitor seed

BHs, how and when these seeds form and how they can grow so rapidly, in less than ~ 1 Gyr, up to few billion solar masses and more.

Different scenarios for BH formation have been proposed so far (see e.g. Rees 1978; Volonteri 2010; Volonteri & Bellovary 2012 for comprehensive reviews). BH seeds with $M_{BH} \sim 10^2$ $M_\odot$ are predicted to form as end products of massive, metal-poor Population III (Pop III) stars (e.g. Madau & Rees 2001; Abel, Bryan & Norman 2002; Heger et al. 2003; Yoshida, Omukai & Hernquist 2008; Latif et al. 2013b; Hirano et al. 2014). Runaway collisions of massive stars during the gravitational collapse of the core of compact star clusters can lead to the formation of intermediate-mass BHs with $M_{BH} \sim 10^3$–10^4 $M_\odot$ (e.g. Tutukov, Shustov & Wiebe 2000; Omukai, Schneider & Haiman 2008; Devecchi & Volonteri 2009; Katz, Sijacki & Haehnelt 2015). In addition, the fast merging of stellar mass BHs in a cluster has been proposed as a possible way to give rise to more massive seeds (Davies, Miller & Bellovary 2011; Lupi et al. 2014). Finally, the formation of more massive, 10^4–10^6 $M_\odot$, seed BHs is predicted to occur via direct collapse of dense, metal-poor gas clouds in haloes with virial temperatures $T_{vir} \geq 10^4$ K which are exposed to a strong H$_2$ photodissociating flux (e.g. Bromm & Loeb 2003; Begelman, Volonteri & Rees 2006; Spaans & Silk 2006; Inayoshi & Omukai 2012; Ferrara et al. 2014;

Inayoshi, Omukai & Tasker 2014). Low metallicity and the suppression of H_2 molecules formation are fundamental requirements for avoiding gas cooling, cloud fragmentation and thus star formation.

It has been suggested that the less massive seeds (Pop III remnants and collapsed stellar clusters) would require a continuous gas accretion close to or above the Eddington limit in order to grow up to few billion solar masses in less than ~ 1 Gyr. For example, Johnson et al. (2013) show that BH seeds as massive as 10^5 $M_\odot$ are required if sub-Eddington accretion and a large radiative efficiency ($\epsilon_r \geq 0.1$) are assumed (see also Volonteri, Silk & Dubus 2015).

Although the conditions in which they can form are met only in very rare environments (e.g. Hosokawa, Omukai & Yorke 2012; Hosokawa et al. 2013; Inayoshi & Haiman 2014; Inayoshi et al. 2014; Yue et al. 2014; Sugimura et al. 2016), direct collapse BHs (DCBHs) have been proposed as a viable scenario to explain high-redshift SMBHs. The formation mechanism, characteristic mass and relevant processes in the direct collapse scenario have been widely investigated in the literature (e.g. Agarwal et al. 2012, 2014, 2015; Johnson et al. 2012; Latif et al. 2013a,b, 2014a; Sugimura, Omukai & Inoue 2014; Glover 2015a,b; Latif & Volonteri 2015).

The work presented in this paper is similar in spirit to what has been done by Petri, Ferrara & Salvaterra (2012) who presented a semi-analytic model for the assembly of high-z SMBHs along a merger history, starting from DCBHs of 10^5 $M_\odot$ and stellar mass BHs of 10^2 $M_\odot$. They show that the final BH mass assembled via both gas accretion and BH–BH mergers strongly depends on the fraction of haloes hosting DCBHs in the merger tree. An $\sim 10^{10}$ $M_\odot$ BH can be obtained if this fraction reaches 100 per cent. However, these authors do not follow the chemical evolution of the host galaxies, and in particular of the metallicity and dust-to-gas ratio of the interstellar medium (ISM).

The aim of this paper is to investigate the relative role of the less massive, Pop III remnant, seed BHs (light seeds) and of the most massive DCBH seeds (heavy seeds) in the formation and evolution of the first SMBHs, taking into account the BH–host galaxy co-evolution. To this aim, we adopt an improved version of the semi-analytic code GAMETE/QSODUST which has been successfully used to investigate the evolutionary scenarios of high-redshift quasars at $z > 5$ (Valiante et al. 2011, 2012, 2014). In particular, together with the mass of the BH, the model well reproduces the properties of the quasars host galaxies such as the star formation rate (SFR), the mass of gas, metals and dust.

As in Valiante et al. (2011) we select as our target the quasar SDSS J1148+5251, observed at redshift $z = 6.4$. This is one of the best studied object at high redshift, hosting a BH mass of $(2–6) \times 10^9$ $M_\odot$ (Barth et al. 2003; Willott, McLure & Jarvis 2003). The other main observed properties of this quasar are summarized in Valiante et al. (2011, 2014).

The paper is organized as follows. In Section 2, we present our approach introducing the model GAMETE/QSODUST and presenting in details the new features implemented for this work. The results are presented in Section 3 where we study the redshift evolution of the BH mass and the birth environment of the seeds predicted by the reference model. In Section 4, we discuss the dependence of the results on the model assumptions and parameters, and we summarize the conclusions in Section 5.

2 SUMMARY OF THE MODEL

Here we briefly introduce GAMETE/QSODUST, the semi-analytic model adopted for this study, focusing on the new features implemented

to investigate the nature of the first seed BHs. We refer the reader to Valiante et al. (2011, 2014) for a full description of the code.

GAMETE/QSODUST is a data constrained model aimed at the study of the formation and evolution of the first quasars and their host galaxies. It is based on the semi-analytic merger tree model GAMETE which was originally developed by Salvadori, Schneider & Ferrara (2007) to investigate the early evolution of the Milky Way and later applied to the Milky Way dwarf satellites (Salvadori, Ferrara & Schneider 2008; Salvadori & Ferrara 2009; Salvadori, Skúladóttir & Tolstoy 2015), to investigate their contribution to the reionization and metal enrichment history of the Local Group (Salvadori et al. 2014), and to explore the connection of damped Lyman α (Lyα) systems with local dwarfs (Salvadori & Ferrara 2012). A two-phase ISM version of GAMETE was successfully adopted as a stellar archaeology tool to investigate the origin of metal-poor low-mass stars in the Milky Way (de Bennassuti et al. 2014; de Bennassuti et al., in preparation).

In its present version, GAMETE/QSODUST enables us to investigate the co-evolution of nuclear BHs and their host galaxies, following their star formation histories and the enrichment of their ISM with metals and dust. The gas reservoir inside each galaxy is regulated by processes of star formation, BH growth and feedback.

We assume that the first SMBHs, observed at $z > 5$, reside in dark matter (DM) haloes of $M_h = 10^{13}$ $M_\odot$ Thus, we first reconstruct the merger tree of such massive haloes, decomposing them into their progenitors, backward in time, following a binary Monte Carlo approach based on the extended Press–Schechter theory (see Valiante et al. 2011 and references therein for details): at each timestep, a halo of mass M_h can either lose mass or lose mass and fragment into two less massive ($\leq M_h/2$) progenitors.

Along the merger history of the DM progenitors, we follow the gradual evolution of the central SMBH and its host galaxy, via both mass accretion and mergers. We define as major mergers haloes merging with mass ratio $\mu > 1/4$, where μ is the ratio of the less massive halo over the most massive companion. In each galaxy, the SFR is assumed to be proportional to the available gas mass and the efficiency at which the gas is transformed into stars is enhanced during major mergers (see Valiante et al. 2011, 2014).

Following Valiante et al. (2011), we assume that in major mergers pre-existing BHs merge in symbiosis with their host galaxies and form of a new, more massive BH. In minor mergers, BHs are unable to spiral in on short time-scales as the merger time-scale is of the order of the Hubble time or longer (see e.g. Tanaka & Haiman 2009). As a result, the least massive BH of the merging pair remains as a satellite and we do not follow its evolution.

We assume Eddington-limited BH growth. The accretion rate is described by the Bondi–Hoyle–Lyttleton (BHL) formula where we introduce a free parameter, α_{BH}, which is commonly adopted to quantify the increased density in the inner regions around the BH (Di Matteo, Springel & Hernquist 2005). A value of $\alpha_{BH} = 50$ is fixed to match the observed SMBH mass of J1148. A fraction of the energy released by supernova (SN) explosions and BH accretion is converted into kinetic energy of the gas in the host galaxy, thus driving gas outflows in the form of winds. In our previous study (Valiante et al. 2012), we show that the BH–host galaxy co-evolution is regulated by quasar feedback, with SN-driven winds providing a negligible contribution to the mass outflow rate, in good agreement with observations of outflowing gas in J1148 (Maiolino et al. 2012; Cicone et al. 2015). The AGN-driven wind efficiency $\epsilon_{w,AGN} = 2.5 \times 10^{-3}$ is fixed to match the observed gas mass in the host galaxy of J1148 (see Section 2.7).

Finally, the ISM of each progenitor galaxy is progressively enriched with metals and dust produced by asymptotic giant branch
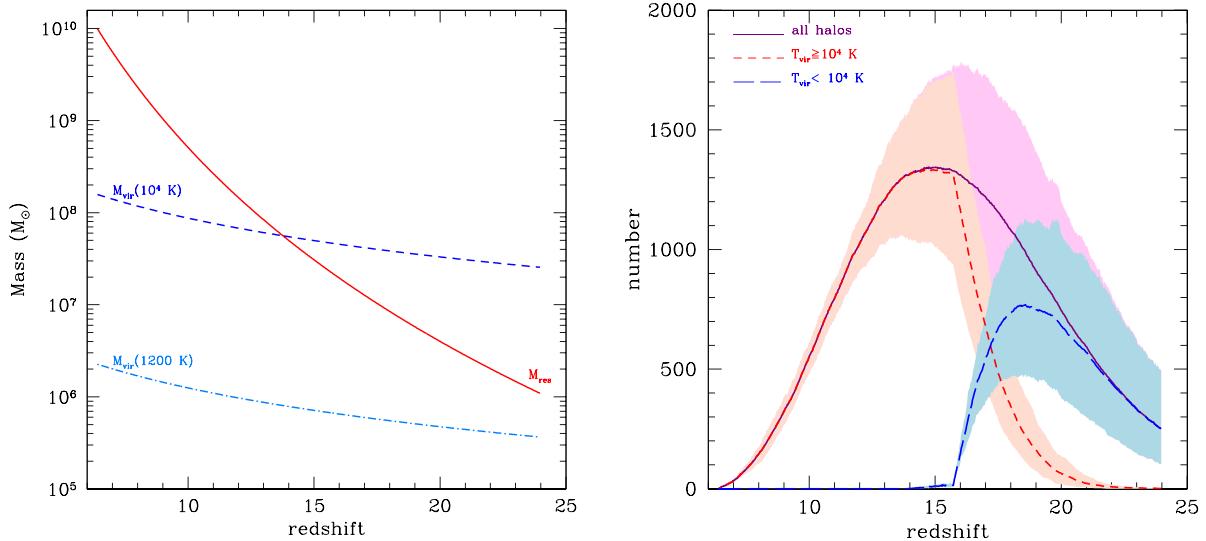
Figure 1. Left-hand panel: redshift evolution of the resolution mass adopted in the merger tree simulations (solid red line) and of the DM halo masses corresponding to a virial temperature of 1200 K (azure dot–dashed line) and 10^4 K (blue dashed line). Right-hand panel: the number of DM haloes as a function of redshift averaged over 10 independent realizations of the merger tree (solid line). Long- and short-dashed lines show the separate contributions of mini-haloes and Lyα haloes (see the text). Shaded regions represent the minimum and maximum values at each redshift.

stars and SNe according to their stellar evolutionary time-scales. Here we adopt the improved version of the chemical evolution module of GAMETE/QSODUST presented in Valiante et al. (2014), where we consistently follow the evolution of metals and dust taking into account the dust life cycle in a two-phase ISM. In hot diffuse gas, dust grains can be destroyed by SN shocks while in cold, dense clouds – where stars form – dust grains can grow by accretion of gas-phase heavy elements.

In the following sections, we describe the new features introduced in the model for the purpose of the present study.

2.1 Resolving mini-haloes

The first collapsed objects where the gas is able to cool and form stars have small masses, $M_{\rm h} \sim 10^{5-6}$ M$_\odot$, and virial temperatures $T_{\rm vir} < 10^4$ K (see e.g. Bromm 2013 for a recent review). To resolve these so-called *mini-haloes*, we simulate the merger trees adopting a minimum mass of

$$M_{\rm res}(z_i) = 10^{-3} M_{\rm h}(z_0) \left(\frac{1 + z_i}{1 + z_0} \right)^{-7.5}, \qquad (1)$$

where $M_{\rm h}(z_0) = 10^{13}$ M$_\odot$ is the host DM halo at redshift $z_0 = 6.4$. The redshift evolution of this resolution mass is shown in the left-hand panel of Fig. 1. This choice enables us to simulate different realizations of the merger tree resolving high-z mini-haloes in a relatively short computational time.

In mini-haloes, which we define here as DM haloes with 1200 K $\leq T_{\rm vir} < 10^4$ K, the primordial gas can cool via rotational transitions of H$_2$ (e.g. Haiman, Thoul & Loeb 1996). DM haloes whose virial temperature exceeds the threshold for efficient atomic line cooling, $T_{\rm vir} \geq 10^4$ K, are instead referred to as Lyα haloes. The number of mini-haloes and Lyα haloes averaged over 10 different merger tree realizations is shown as a function of redshift in the right-hand panel of Fig. 1. As expected, at $z \gtrsim 17$ mini-haloes represent the dominant population among DM progenitors. Their number decreases at lower redshift down to $z \sim 14$, below which the halo population is completely dominated by more massive systems. This

is a consequence of the redshift evolution of the assumed resolution mass which exceeds the minimum mass of Lyα haloes at these redshifts.[1]

2.2 UV radiation

The radiation emitted by stars and accreting BHs gradually builds up a cosmic ultraviolet (UV) background. Since we reconstruct the merger history of a single biased, high-density region at $z > 6$, here we refer to UV background as the cumulative emission coming from all the progenitor galaxies of the $M_{\rm h} = 10^{13}$ M$_\odot$ DM halo within its comoving volume at the turn-around radius, $V_{\rm com} = 50$ Mpc^3.

Radiative feedback effects have a fundamental role in the history of star and BH seed formation. Photons in the Lyman–Werner (LW) band, [11.2–13.6] eV, can easily dissociate H$_2$ molecules, suppressing cooling and star formation in metal-poor mini-haloes (e.g. Haiman & Loeb 1997; Haiman, Rees & Loeb 1997; Omukai & Nishi 1999; Machacek, Bryan & Abel 2001; Omukai 2001). Even a moderate LW flux can lead to an increase of the minimum mass required for DM haloes to host star formation (see Appendix A).

The increased gas temperature in photoionized regions leads to an increase of the cosmological Jeans mass. As a result, gas accretion on to low-mass DM haloes is suppressed in ionized regions, while the internal gas in existing low-mass haloes will be photoevaporated (e.g. Barkana & Loeb 1999; Shapiro, Iliev & Raga 2004; Sobacchi & Mesinger 2013).

The cumulative flux (in units of erg cm^{-2} s^{-1} Hz^{-1} sr^{-1}) at the observed frequency $\nu_{\rm obs}$ and redshift $z_{\rm obs}$ is computed as (e.g. Haardt

---

[1] In other words, we are not able to resolve mini-haloes at redshift $z < 14$ due to the chosen resolution mass threshold. This does not affect our results because at these z radiative feedback has already suppressed star and BH formation in all haloes below a virial temperature of 10^4 K. This will be discussed in Section 3.

& Madau 1996)

$$J(\nu_{\rm obs}, z_{\rm obs}) = \frac{(1 + z_{\rm obs})^3}{4\pi} \int_{z_{\rm obs}}^{z_{\rm max}} {\rm d}z \, c \left| \frac{{\rm d}t}{{\rm d}z} \right| \epsilon(\nu_z, z) \, {\rm e}^{-\tau_{\rm H_2}(\nu_{\rm obs}, z_{\rm obs}, z)}, \tag{2}$$

where $\tau_{\rm H_2}$ is the H_2 optical depth in the LW band and $\epsilon(\nu_z, z)$ is the comoving emissivity, namely the monochromatic luminosity per unit comoving volume (erg s^{-1} Hz^{-1} cm^{-3}), in the LW band at redshift z. The redshift $z_{\rm max}$ represents the highest redshift from which an LW photon emitted by a source at $z > z_{\rm obs}$ can reach the observer at $z_{\rm obs}$ before being redshifted at lower frequencies, outside the LW range, into an H Lyman resonance line. In the dark screen approximation, this redshift can be defined as $(1 + z_{\rm max})/(1 + z_{\rm obs})$ $= \nu_i/\nu_{\rm obs}$ (see e.g. Haiman et al. 1997; Haiman, Abel & Rees 2000) being ν_i the first Lyman line frequency above the observed one.

In general, $\tau_{\rm H_2}$ depends on H_2 number density, on the line profile and on the probability that the molecule is dissociated after a transition. It can reach values $\tau_{\rm H_2} \geq 3$ (Ciardi, Ferrara & Abel 2000; Ricotti, Gnedin & Shull 2001) leading to a reduction in the LW background flux of about one order of magnitude. Following Ahn et al. (2009) we compute the intergalactic absorption averaged over the LW band using the modulation factor described by the fitting formula:

$$ {\rm e}^{-\tau_{\rm H_2}} = \begin{cases} 1.7 \, {\rm e}^{-(r_{\rm cMpc}/116.29\alpha)^{0.68}} - 0.7 & {\rm if} \; r_{\rm cMpc}/\alpha \leq 97.39 \\ 0 & {\rm if} \; r_{\rm cMpc}/\alpha > 97.39 \end{cases} \tag{3}$$

where $r_{\rm cMpc}$ is the distance between the emitting source, at redshift z, and the observer at redshift $z_{\rm obs}$, expressed in units of comoving Mpc:

$$r_{\rm cMpc} = -\int_{z_{\rm obs}}^{z} \frac{c \, {\rm d}z}{H(z)} \tag{4}$$

with $H(z) = H_0[\Omega_{\rm M}(1 + z)^3 + \Omega_\Lambda]^{1/2}$. The scaling factor α in equation (3) is defined as

$$\alpha = \left(\frac{h}{0.7} \right)^{-1} \left(\frac{\Omega_{\rm M}}{0.27} \right)^{-1/2} \left(\frac{1 + z}{21} \right)^{-1/2}. \tag{5}$$

The resulting average attenuation of the UV flux increases with increasing comoving ratio $r_{\rm cMpc}/\alpha$, approaching zero when $r_{\rm cMpc} = 97.39\alpha$ which is the maximum distance from which the observer can see LW photons emitted by a source at redshift z, the so-called LW horizon (see fig. 3 of Ahn et al. 2009).

In what follows, we call $J_{\rm LW}$ the LW background flux in units of 10^{-21} erg cm^{-2} s^{-1} Hz^{-1} sr^{-1} and we compute it at the central frequency of the LW band using equations (2)–(5).

Following Salvadori et al. (2014), the time evolution of the filling factor of ionized regions is computed as

$$\dot{Q}_{\rm HII}(z) = f_{\rm esc} \dot{n}_\gamma / n_{\rm H} - \alpha_{\rm B} \, C \, n_{\rm H} \, (1 + z)^3 \, Q_{\rm HII}, \tag{6}$$

where $f_{\rm esc} = 0.1$ is the escape fraction of ionizing photons, $\dot{n}_\gamma = \sum_i \dot{N}_{\gamma, i}/V_{\rm com}$ is the total production rate of ionizing photons per unit volume summed over all the emitting sources, $n_{\rm H} = X_{\rm H} \, n_{\rm IGM}$ is the comoving hydrogen number density in the intergalactic medium (IGM), $n_{\rm IGM}$ is the IGM gas number density and $X_{\rm H} = 0.76$ is the hydrogen mass fraction. In the right-hand side of equation (6), $\alpha_{\rm B} = 2.6 \times 10^{-13}$ cm^3 s^{-1} is the hydrogen recombination rate and $C = 3$ is the clumping factor.

At each given redshift, the total LW emissivity and ionizing photon rate are computed summing over all the emitting sources both stars and accreting BHs. For Pop III stars, we use the mass-dependent emissivities given by Schaerer (2002) for $Z = 0$ stars with

no mass-loss (see tables 4 and 6 of the original paper). For Pop II/I stars, we compute the metallicity and age-dependent emissivities using the Bruzual & Charlot (2003) population synthesis model. We assume that the stars form in a single burst with a Salpeter initial mass function (IMF) in the mass range [0.1–100] M$_\odot$. For accreting BHs, we compute the LW and ionizing photon production rates by modelling the spectral energy distribution (SED) as a classic multicolour disc spectrum up to $kT_{\rm max} \sim 1$ keV $(M_{\rm BH}/M_\odot)^{-1/4}$ (Shakura & Sunyaev 1973), and a non-thermal power-law component with spectral slope $L_\nu \propto \nu^{-\alpha}$, with $\alpha \approx 2$ at higher energies (Shakura & Sunyaev 1973; Sazonov, Ostriker & Sunyaev 2004).

2.3 Star formation rate

In each progenitor galaxy, the star formation rate is computed as

$$ {\rm SFR} = f_{\rm cool} \, M_{\rm ISM} \, (\epsilon_{\rm quies} + \epsilon_{\rm burst})/\tau_{\rm dyn}, \tag{7}$$

where $M_{\rm ISM}$ is the gas mass, $\epsilon_{\rm quies} + \epsilon_{\rm burst}$ is the total star formation efficiency accounting for both quiescent and merger-driven episodes of star formation. Following Valiante et al. (2011), we take $\epsilon_{\rm quies} = 0.1$ and $\epsilon_{\rm burst} = 8$ for equal-mass mergers, with a modulation that depends on the mass ratio of the merging pairs (see equation 11 and table 2 in Valiante et al. 2011). Finally, the quantity $f_{\rm cool}$ quantifies the reduced cooling efficiency of mini-haloes with respect to Lyα haloes. Hence, we assume $f_{\rm cool} = 1$ in progenitor systems with $T_{\rm vir} \geq 10^4$ K whereas in mini-haloes this parameter quantifies the mass fraction of gas that can cool in one dynamical time and it depends on the virial temperature, redshift, gas metallicity and intensity of the LW background. The computation of $f_{\rm cool}$ is described in Appendix A.

2.3.1 Photoheating feedback

To account for the effects of the increased gas temperature in photoionized regions, we assume that star formation is suppressed, i.e. $(\epsilon_{\rm quies} + \epsilon_{\rm burst}) = 0$, in haloes with virial temperature below the temperature of the IGM. Hence, we neglect the hydrodynamic response of the gas (see Sobacchi & Mesinger 2013) and we assume a feedback model where star formation is suppressed instantaneously when $T_{\rm vir} < T_{\rm IGM}$. The mean IGM temperature is computed taking into account the volume filling factor of ionized regions, $T_{\rm IGM} = Q_{\rm HII} \, T_{\rm reio} + (1 - Q_{\rm HII}) \, T_{\rm gas}$, where $T_{\rm reio} = 2 \times 10^4$ K is the assumed post-reionization temperature and $T_{\rm gas} = 170 \, (1 + z)^2$.

2.3.2 Photodissociating feedback

Suppression of H_2 cooling and star formation in mini-haloes due to photodissociation by LW photons is taken into account through the parameter $f_{\rm cool}$ in equation (7), whose calculation is presented in Appendix A. Depending on the halo virial temperature, redshift, gas metallicity and intensity of the LW background, we compare the cooling time and the free-fall time and quantify the mass fraction of gas that is able to cool and form stars. We find that in the presence of an LW background, the cooling efficiency is rapidly suppressed in mini-haloes. In fact, when $J_{\rm LW} \lesssim 1$, $f_{\rm cool} \neq 0$ only in mini-haloes at $z \gtrsim 20$ or if the gas is already metal-enriched to $Z \gtrsim 0.1 \, Z_\odot$. For more details, we refer the reader to Appendix A and Figs A1–A4.

2.4 Stellar IMF

Currently, there are no direct observational constraints on the IMF of the first generation of stars. Theoretical studies do not yet provide
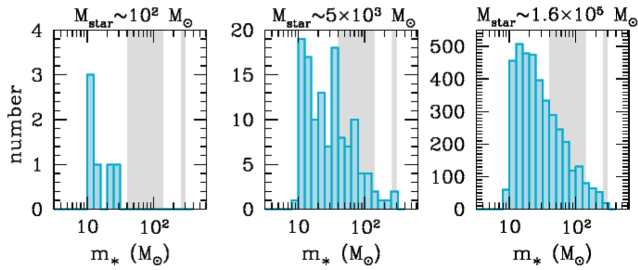
Figure 2. Examples of the mass distribution of Pop III stars emerging from stochastic sampling of the IMF in three different haloes (see the text). The total stellar mass formed is $10^2\,M_\odot$ (left-hand panel), $\sim 5 \times 10^3\,M_\odot$ (middle panel) and $\sim 1.6 \times 10^5\,M_\odot$ (right-hand panel). Grey shaded regions indicate the mass range leading to BH remnants.

a firm determination of the stellar mass spectrum emerging from the first star-forming regions (see e.g. Bromm 2013 and Glover 2013 for comprehensive reviews). Recent numerical studies suggest that – depending on their formation environment – Pop III stars can have masses varying from tens to thousands of solar masses, with a distribution that peaks around few tens to few hundreds of solar masses (e.g. Hosokawa et al. 2011; Hirano et al. 2014, 2015; Susa, Hasegawa & Tominaga 2014).

Following de Bennassuti et al. (2014), we assume that Pop III stars form according to a Larson IMF (Larson 1998),

$$\Phi(m_*) \propto m_*^{\alpha-1}\,e^{-m_*/m_{\rm ch}}, \qquad (8)$$

with $\alpha = -1.35$, $m_{\rm ch} = 20\,M_\odot$ and $10\,M_\odot \leq m_* \leq 300\,M_\odot$. During each star formation episode, we stochastically sample the IMF until we reach the total stellar mass formed[2] (see also de Bennassuti et al., in preparation). In Fig. 2, we show three examples of the mass distribution of Pop III stars emerging from a star formation episode where the total stellar mass formed is $M_{\rm star} \sim 10^2\,M_\odot$ (left-hand panel), $\sim 5 \times 10^3\,M_\odot$ (middle panel) and $\sim 1.6 \times 10^5\,M_\odot$ (right-hand panel). The stellar population shown in the left-hand panel is representative of the conditions that apply in small-mass mini-haloes. Only six stars are formed with masses in the range $[10-30]\,M_\odot$. In larger mass haloes, as shown in the middle and right-hand panels, the mass range that is populated is extended towards larger stellar masses.

When the metallicity in star-forming regions is $Z_{\rm ISM} \geq Z_{\rm crit}$, where $Z_{\rm crit}$ is the critical metallicity for low-mass star formation (Bromm et al. 2001; Schneider et al. 2002, 2003), we assume that Pop II stars form in the stellar mass range $[0.1-100]\,M_\odot$ according to a Larson IMF with $m_{\rm ch} = 0.35\,M_\odot$. In what follows, we adopt $Z_{\rm crit} = 10^{-3.8}$ $Z_\odot$ and we discuss the impact of assuming a dust-driven transition at lower $Z_{\rm crit}$ (Omukai et al. 2005; Schneider et al. 2012a).

2.5 Light BH seed formation

Light BH seeds form as remnants of Pop III stars. Here we assume that stars with masses in the range $[40-140]\,M_\odot$ and $\geq 260\,M_\odot$ do not explode as SNe and directly collapse to BHs (Heger & Woosley 2002). The number and masses of BH remnants depend on the frequency with which these mass ranges are sampled when Pop III stars form and stochastically populate the IMF (see the previous section). In the two haloes shown in the middle and right-hand panels of Fig. 2, the stochastic sampling selects 124 and 3900

stars. The shaded regions in the same figure indicate the mass range leading to BH remnants. In small mini-haloes, light BH seeds are very rare (see the left-hand panel).

The subsequent evolution of newly formed BHs depends on their mass. As discussed by Volonteri (2010), lighter BHs are not expected to settle at the centre but rather wander through the host galaxy, interacting with stars. For this reason, we select as a light BH seed the most massive BH remnant.[3] We discuss the implications of this assumption in Section 4.

2.6 Heavy BH seed formation

Fragmentation of gas clouds, and thus star formation, is prevented in Lyα haloes ($T_{\rm vir} \geq 10^4$ K) in which the ISM metallicity is sub-critical ($Z_{\rm ISM} < Z_{\rm cr}$) and the LW background is strong enough to photodissociate H_2 (Omukai et al. 2008). The latter condition is usually expressed as $J_{\rm LW} > J_{\rm cr}$, where $J_{\rm cr}$ is the critical value in units of 10^{-21} erg cm^{-2} s^{-1} Hz^{-1} sr^{-1}. If all the above conditions are simultaneously satisfied, the collapse proceeds almost isothermally thanks to atomic H line cooling, avoiding fragmentation into smaller clumps. This process leads to the formation of a single BH with mass in the range $[10^4-10^6]\,M_\odot$, which we call heavy BH seed, in some cases through an intermediate phase of supermassive star formation (see e.g. Hosokawa et al. 2012, 2013 for more details). Recently, Ferrara et al. (2014) investigated the mass spectrum of heavy BH seeds and found that their masses range between $\sim 5 \times 10^4$ and $\sim 2 \times 10^6\,M_\odot$ (see also Volonteri & Begelman 2010).

Following these studies, we assume that heavy BH seeds form with an average mass of $10^5\,M_\odot$ in Lyα haloes with sub-critical metallicity and super-critical LW background.

The exact value of $J_{\rm cr}$ is still a matter of debate. Its value depends on whether sufficient H_2 to cool the gas within a free-fall time is formed before it is collisionally dissociated at $\sim 10^4$ cm^{-3}, and depends on the SED of the sources of radiation (Omukai 2001; Oh & Haiman 2002; Bromm & Loeb 2003; Omukai et al. 2008; Agarwal et al. 2012, 2015; Latif et al. 2014a; Sugimura et al. 2014, 2016). In addition, Lyα haloes can be exposed to intense local radiation, which exceeds the background level, in biased, dense regions of the Universe, and close to star-forming galaxies (Dijkstra et al. 2008; Tanaka & Haiman 2009; Dijkstra, Ferrara & Mesinger 2014). Additional complications come when H_2 self-shielding is taken into account (Shang, Bryan & Haiman 2010; Hartwig et al. 2015) and when the presence of X-ray or ionizing radiation increases the free electron fraction, favouring the formation of H_2 (Inayoshi & Omukai 2011; Johnson et al. 2014; Yue et al. 2014; Inayoshi & Tanaka 2015). As a result, values of $J_{\rm cr}$ between ~ 30 and $\sim 10^4$ have been proposed and used to estimate the number density of heavy seeds. In particular, $J_{\rm cr} > 500$–10^3 and up to 10^4–10^5 is always required to enable the direct collapse mechanism in 3D numerical simulations to produce supermassive stars with mass 10^4–$10^5\,M_\odot$ (Latif et al. 2014b; Regan, Johansson & Wise 2014; Latif & Volonteri 2015). Here we adopt a reference value of $J_{\rm cr} = 300$ and we discuss the implications of this assumption in Section 4.

---

[2] We have tested that the IMF is fully reconstructed in the $[10-300]\,M_\odot$ mass range when the total stellar mass formed is $M_{\rm star} > 10^6\,M_\odot$.

[3] In the three examples shown in Fig. 2, we do not assign any light BH seed to the population represented by the left-hand panel and only one light BH seed in the other cases, taken to be the most massive BH remnant among the 2 (15) BHs of $\sim [260-300]\,M_\odot$ formed in the middle (right) panel.
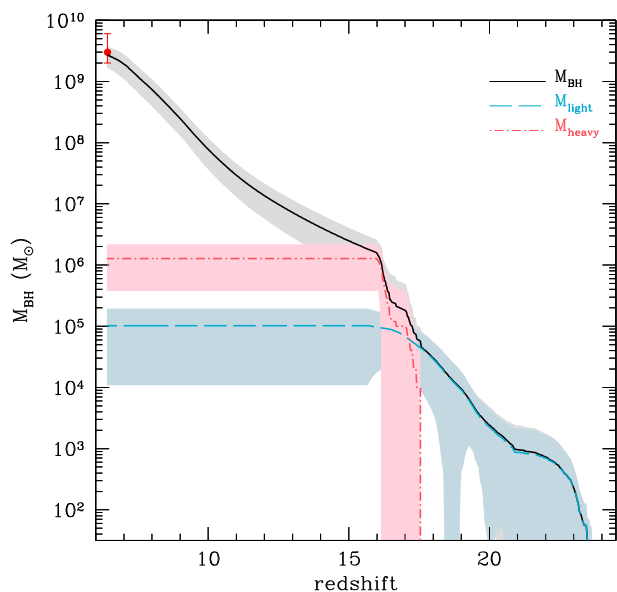
Figure 3. BH mass as a function of redshift. The black solid line represents the total mass in BHs growing by gas accretion and mergers with other BHs, while the blue dashed and the red dot–dashed lines show the contribution of the light and heavy seed BHs, respectively (without gas accretion). Each line is the average over 10 different merger tree realizations with the shades indicating 1σ dispersion.

3 RESULTS

In this section, we present the main results of our study. In the same spirit of Valiante et al. (2011, 2014), we follow the formation of an SMBH with a mass of $\sim(2–6) \times 10^9$ $M_\odot$ at redshift $z = 6.4$, similar to the one expected to power the bright quasar J1148 (Barth et al. 2003; Willott et al. 2003; De Rosa et al. 2011). In what follows, we present the results averaged over 10 independent realizations of the merger tree of a 10^{13} $M_\odot$ DM halo. However, in order to explore the dependence of some results on the merger history, we also discuss the properties of individual merger trees.

3.1 Evolution of the BH mass

In Fig. 3, we show the predicted evolution of the total BH mass in a merger tree as a function of redshift. For each merger tree, we consider the contribution of BH progenitors to the total BH mass at each redshift. We classify as BH progenitors only those BHs which do not become satellites at any stage of the merger tree and whose mass will be inherited by the final SMBH at $z = 6.4$.[4] The free parameters of the model have been selected to reproduce an SMBH mass of $\sim3 \times 10^9$ $M_\odot$ at $z = 6.4$, in good agreement with that expected for quasar J1148 (red data point in Fig. 3). In the same figure, we also show the separate contribution of light (blue dashed line) and heavy (red dot–dashed line) BH seeds to the total BH mass at different epochs.

---

[4] For each merger tree, we follow backward in time the evolution of the SMBH. At each minor merger event, we cut the branch of the tree of the lighter, satellite progenitor BH and we only follow the branch of the most massive one. At each major merger event, we continue to follow both branches of the progenitor BHs. This procedure allows us to reconstruct a posteriori the sample of BH progenitors whose masses directly contribute to the final SMBH mass at $z = 6.4$.

Light seeds-dominated regime. At high redshift ($z \gtrsim 18$), BH growth is dominated by the formation of light seeds. Their rate of formation is strongly regulated by photodissociating feedback which inhibits Pop III star formation in mini-haloes. The total mass from BH light seeds rapidly grows in time, reaching, on average, a maximum value of $\sim10^5$ $M_\odot$ at $z \sim 15.5$, below which their formation is suppressed by metal enrichment.

Heavy seeds-dominated regime. Heavy seeds start to form at redshift $z \lesssim 18$ and dominate the evolution of the BH mass for a brief but significant period of time. In fact, they rapidly grow in number, and by $z \sim 15.5$ their contribution to the total BH mass is, on average, $\sim1.3 \times 10^6$ $M_\odot$, more than one order of magnitude larger than that of light BH seeds. Not surprisingly, the rise of heavy seeds marks the fall of light seeds. In fact, Lyα haloes with $Z < Z_{cr}$ either form Pop III stars, hence light BH seeds (when $J_{LW} < J_{cr}$), or form heavy seeds (when $J_{LW} \geq J_{cr}$).

Accretion-dominated regime. At $z \lesssim 16$, BH growth is dominated by gas accretion. In fact, at this epoch, the progenitor galaxies are all enriched to $Z \geq Z_{cr}$ preventing the formation of both light and heavy seeds. Overall, gas accretion provides the dominant contribution to the final SMBH mass at $z = 6.4$, in agreement with Valiante et al. (2011).[5] This is a consequence of the strong BH mass dependence of the BHL accretion law, which leads to runaway BH growth.

In our reference model, a total of ~4800 light and ~100 heavy seeds are formed, on average, at $z \gtrsim 16$. However, only ~13 per cent of these seeds (~620 light and ~13 heavy) are BH progenitors, because a dominant fraction is lost along minor branches of the merger tree and become satellites.

In Fig. 4, we show the BH progenitor formation redshifts and birth masses. Light BH seeds start forming at $z \sim 24$ although their number increases considerably at $z \lesssim 20$, with a peak at $z \sim 17$ followed by a rapid decline. This redshift distribution reflects the properties of their birth environments. At the highest z, light BH seeds form in mini-haloes, whose star formation efficiency is low and prone to photodissociating feedback. Their birth mass distribution shows that the largest number of light BH seeds is concentrated in the most massive bin, with ~240 BHs (~40 per cent of the total) with mass in the range [260−300] $M_\odot$, while the remaining are almost equally distributed between 40 and 140 $M_\odot$ (see the right-hand panel). On the other hand, heavy seed BH progenitors form, on average, over a very narrow redshift range, at $15.5 \lesssim z \lesssim 18$, with a peak at $z \sim 16.5$ that is slightly shifted with respect to that of light seeds, followed by a sharp decline. This sudden appearance and decline of heavy seeds is a consequence of their tight birth environmental conditions which are satisfied only by a relatively small number of haloes and over a very limited period of time, as will be clarified in the following section.

3.2 Birth environment of SMBH seeds

The results presented in the previous section show how the mass growth of SMBHs at $z > 6$ depends on a complex interplay between radiative and chemical feedback processes that shape the birth environment of light and heavy BH seeds. Since SMBHs at $z > 6$ form in biased regions of the Universe, the intensity of the LW background,

---

[5] In Valiante et al. (2011), gas accretion dominates the evolution of the BH mass at $z \lesssim 11$. In the present model, gas accretion starts to dominate at an earlier redshift. The difference with Valiante et al. (2011) is due to the different merger histories (which now include mini-haloes) and BH seeding prescription.
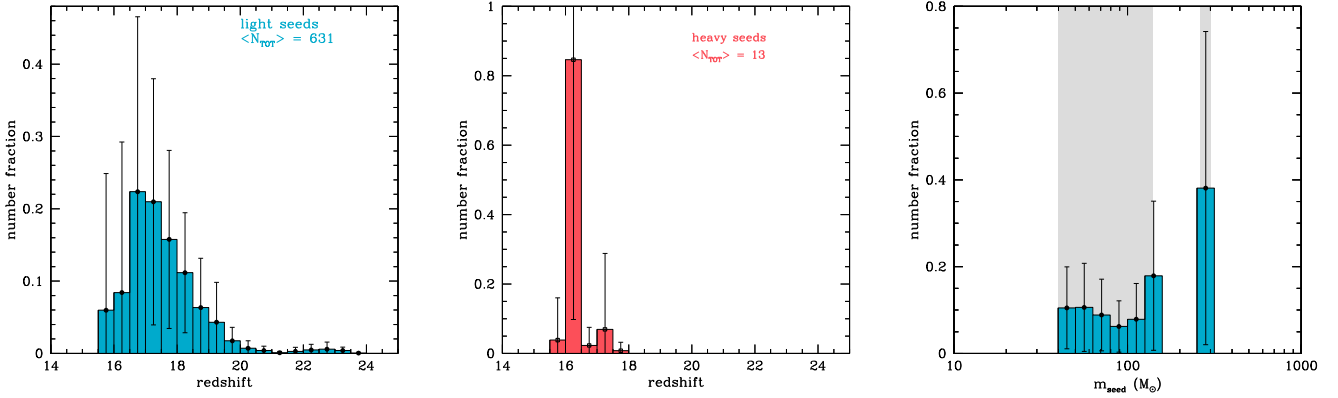
Figure 4. Distribution of formation redshift of light (left-hand panel) and heavy seeds (central panel). The right-hand panel shows the distribution of birth masses for light seeds only as heavy seeds are all assumed to have a mass of 10^5 M$_\odot$. Histograms and data points show the average over 10 different merger tree realizations with 1σ error bars.
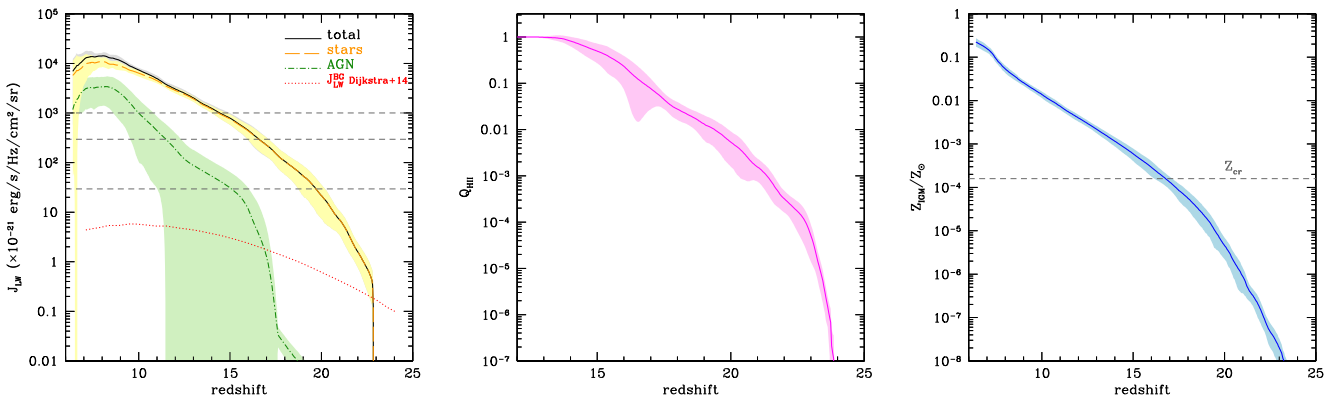

Figure 5. Left-hand panel: redshift evolution of the total LW background flux (black solid line). Green dot–dashed and yellow dashed lines indicate the contribution of accreting BHs (AGNs) and stars, respectively. The three horizontal lines indicate three different critical values $J_{\rm cr} = 30, 300$ and 10^3 (see the text for details). For comparison, we also show the cosmic mean LW background predicted by Dijkstra et al. (2014, dotted line). Middle panel: volume filling factor of ionized hydrogen regions (H II) as a function of redshift. Right-hand panel: redshift evolution of the metallicity of the IGM in which haloes are embedded. The horizontal line shows the critical metallicity for Pop III/II transition adopted in the reference model. In all panels, lines indicate the average values over 10 different merger tree realizations with shades representing the 1σ dispersion.

the volume filling factor of ionized regions and the gas metallicity, which set the relative strength of feedback processes, are expected to be different from the cosmic mean values at the same redshift.

The left-hand panel of Fig. 5 shows the relative contribution of accreting BHs (AGNs, green dot–dashed line) and stellar emission (yellow dashed line) to the LW background (black solid line). At all redshifts, the LW emission is dominated by star formation. The intensity of the LW background increases very rapidly, exceeding values of $J_{\rm cr} = 30, 300$ and 10^3 (marked by the horizontal lines), on average, at $z \sim 20, 16.5$ and 15, with some dispersion among different merger histories (see Section 3.3). In the same figure, we also show, for comparison, the cosmic mean LW background predicted by Dijkstra et al. (2014).

The central panel of Fig. 5 shows the evolution of the volume filling factor of ionized regions. We find that $Q_{\rm HII} \sim 1$ at $z \lesssim 14$, consistent with the expectations from the rapid increase of the UV background intensity.

Finally, in the right-hand panel of Fig. 5, we present the redshift evolution of the metallicity of the IGM, the medium in which all haloes are embedded. This metallicity, $Z_{\rm IGM}$, increases as mechanical feedback, in the form of galaxy-scale winds driven by the SNe

and AGNs, ejects metal-enriched gas out of the galaxies, enriching the surrounding medium. The horizontal line indicates the critical metallicity for low-mass star formation that we have adopted in the reference model, $Z_{\rm cr} = 10^{-3.8}$ Z$_\odot$. The average IGM metallicity exceeds this critical value at $z \lesssim 17$, with some dispersion among different merger histories.

The effects of radiative feedback on the environment where light and heavy BH seeds form are summarized in Fig. 6, which shows the redshift evolution of the minimum halo mass for star formation (black solid line). At high redshifts, the minimum halo mass rapidly increases as a consequence of photodissociating feedback, reaching the minimum mass of Lyα haloes (short-dashed line) already at $z \sim 20$, on average. Hence, as was anticipated in Section 3.1, the dominant fraction of light BH seeds form in Lyα haloes which are less vulnerable to photodissociating feedback. Within $16 \lesssim z \lesssim 20$ Lyα haloes with masses $M_{\rm h} \sim (3-5) \times 10^7$ M$_\odot$ and sub-critical metallicity can either form light or heavy BH seeds depending on the intensity of $J_{\rm LW}$. When $z \lesssim 16$, the minimum mass for star formation increases as a consequence of photoheating feedback and achieve the adopted minimum mass for star formation in ionized regions, $M_{\rm h} \gtrsim 2 \times 10^8$ M$_\odot$ (dot–dashed line), by $z \sim 13$, when the
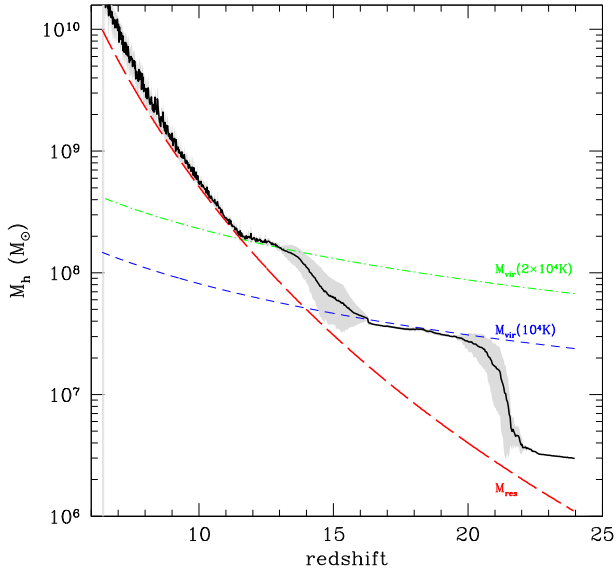
Figure 6. Average minimum halo mass for star-forming as a function of redshift (black solid line). The line indicates the average over 10 different merger histories and the shaded region shows the 1σ dispersion. For comparison, we also show the resolution mass of the merger trees (red long-dashed line), the minimum mass of Lyα haloes (with $T_{vir} = 10^4$ K, blue short-dashed line) and the adopted minimum mass for star formation in ionized regions (with $T_{vir} = 2 \times 10^4$ K, green dot–dashed line).

IGM is fully ionized. The figure also shows that the minimum mass for star formation depends on the adopted resolution mass only at $z \lesssim 11$, when the epoch of BH seed formation is already terminated. Hence, the results are independent of the mass resolution of the merger trees.

Finally, to quantify the effect of chemical feedback on heavy BH seed formation, we compute their occurrence ratio, defined as the number of progenitor haloes which satisfy the conditions $J_{LW} > J_{cr}$ and $Z < Z_{cr}$ divided by the number of progenitor haloes with $J_{LW} > J_{cr}$. When averaged over 10 independent merger histories, we find the occurrence ratio at $z > 15$ to be ~ 5 per cent, meaning that chemical feedback plays a dominant role.

3.3 Dependence on the hierarchical history

One of the advantages of a semi-analytical model is that it allows one to run independent merger tree simulations of the same quasar.

In Fig. 7, we show the evolution of the BH mass and the contribution of light and heavy seeds as a function of redshift for 10 different merger trees. In 9 out of 10 runs, the final BH mass is in very good agreement with the data. The only exception is the simulation shown in panel (e), where only light BH seeds form. This supports the conclusion that, as long as gas accretion is assumed to be Eddington-limited, heavy BH seeds are required to grow an SMBH at $z > 6$.

The relative contribution of light and heavy BH seeds depends on the individual merger tree. Even when light BH seeds start to form at $z \gtrsim 20$ (see panels a, b, f, g and h), their total mass does not exceed $\sim 10^5$ M$_\odot$ and it is comparable to the mass of one single heavy BH seed. Only between ~ 3 and ~ 30 heavy BH seeds are required to grow an SMBH by $z \sim 6.4$, and their total mass ranges between $\sim 3 \times 10^5$ and $\sim 3 \times 10^6$ M$_\odot$.

It is interesting to investigate in more details why no heavy BH seed is formed in the simulation shown in panel (e). We compare the
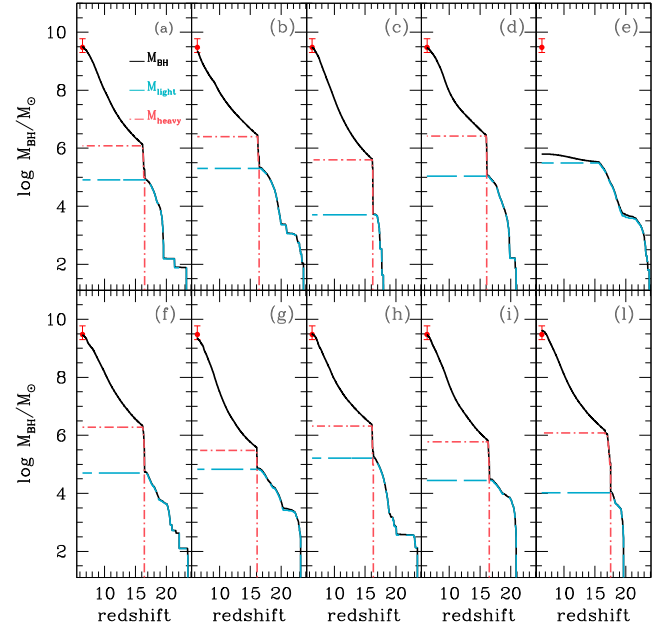

Figure 7. Evolution of the BH mass as a function of redshift for 10 different merger trees. Black solid lines show the total BH mass, while blue dashed and red dot–dashed lines represent the contribution of light and heavy seeds, respectively, without gas accretion.
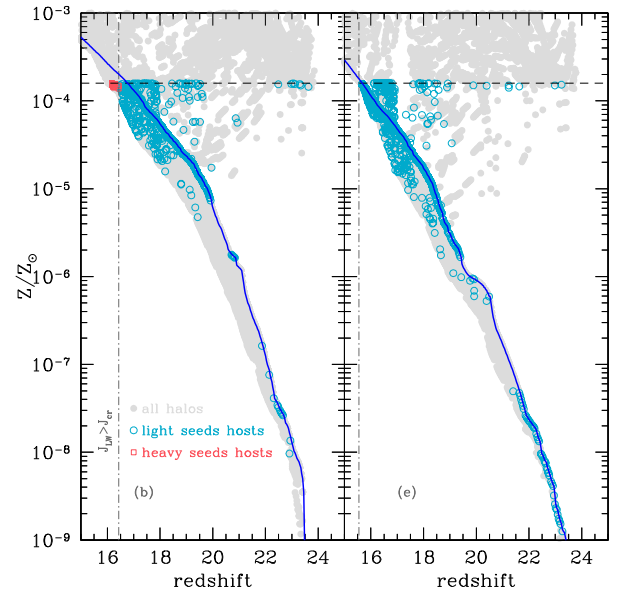

Figure 8. Metallicity as a function of redshift of all the progenitor haloes (grey points) in two merger tree simulations (b, left-hand panel) and (e, left-hand panel) shown in Fig. 7. Open blue circles and red squares indicate the progenitors where light and heavy BH seeds form. In each panel, the solid line is the mean IGM metallicity, the horizontal dashed line is the value of Z_{cr} and the vertical dot–dashed line is the redshift at which $J_{LW} > J_{cr}$.

properties of this simulation with the one shown in panel (b), which is characterized by a similar high-z evolution of the light BH seed mass. In Fig. 8, we show the metallicity of all progenitor haloes in the two simulations (grey points) as a function of redshift. The solid line is the mean metallicity of the IGM and open blue circles (red squares) represent progenitor haloes hosting light (heavy) BH seeds. Light BH seeds form in haloes with $Z < Z_{cr}$, where the
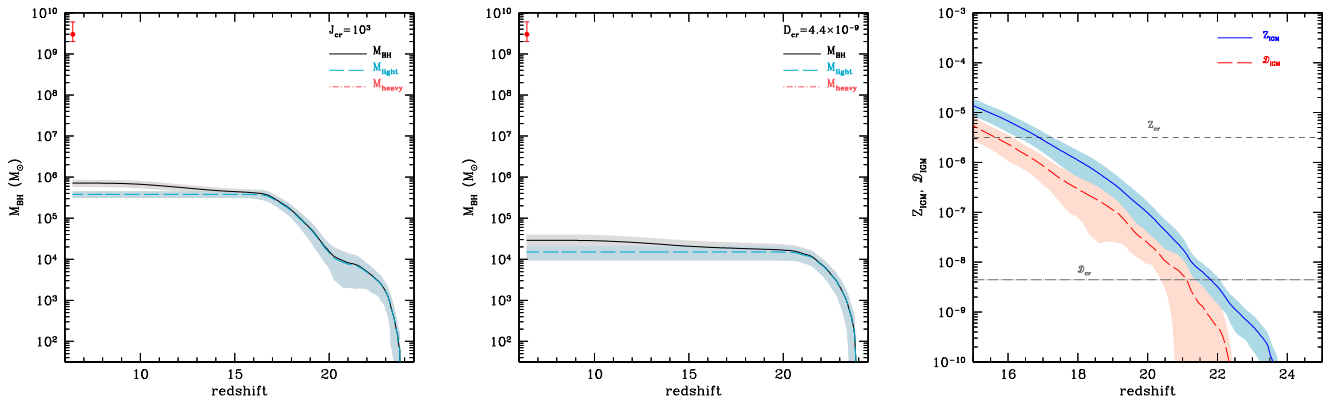
Figure 9. Same as in Fig. 3 but assuming $J_{cr} = 10^3$ (left-hand panel) and a dust-driven transition to Pop II star formation occurring at $\mathcal{D}_{cr} = 4.4 \times 10^{-9}$ (middle panel). In the right-hand panel, we show the average metallicity (blue solid line) and dust-to-gas ratio (red dashed line) of the IGM. Horizontal dashed (dot–dashed) line indicates Z_{cr} in absolute units and $\mathcal{D}_{cr}$, respectively. In all panels, the curves are averages over 10 merger tree realizations with shades representing the 1σ dispersion.

value corresponding to Z_{cr} in the reference model is shown by the horizontal dashed line. As expected, heavy seeds form only in a small number of haloes of simulation (b), where $Z < Z_{cr}$ and $J_{LW} > J_{cr}$ (the redshift at which this condition is satisfied is indicated by the vertical dot–dashed line).

The redshift and metallicity distribution of progenitor haloes is different in the two simulations. Newly virialized progenitor haloes have the same metallicity of the IGM, while in others the metallicity can be significantly smaller or larger. At $z \lesssim 20$, Z_{IGM} is slightly smaller in simulation (e) and there is a smaller fraction of haloes with $Z < Z_{IGM}$, meaning that self-enrichment is more efficient than in simulation (b). In addition, the LW background intensity becomes larger than J_{cr} at a lower redshift in simulation (e), $z \sim 15.5$ instead of $z \sim 16.5$. As a result, there is no single progenitor halo where the conditions for heavy BH seed formation are satisfied.

4 DISCUSSION

The results of the reference model depend on a number of assumptions whose importance is critically discussed below.

4.1 Dependence on J_{cr}

The critical intensity of the LW background that enables the collapse of gas in metal-poor Lyα haloes is still highly debated. Here we discuss the consequences of increasing J_{cr} to 10^3.

Although the LW background can reach very large values in the biased region that we are simulating, on average it exceeds $J_{cr} = 10^3$ at $z \lesssim 14.5$ (see the left-hand panel in Fig. 5), when all progenitor haloes have been already enriched above the critical metallicity for Pop II star formation. Lyα haloes with $Z < Z_{cr}$ and $300 \lesssim J_{LW} \lesssim 10^3$ now host Pop III star formation and no single heavy BH seed forms.

The redshift evolution of the total BH mass is shown in the left-hand panel of Fig. 9. The growth of the BH is strongly suppressed and $M_{BH} \lesssim 10^6 \, M_\odot$ at $z \sim 6.4$. In fact, despite the larger number of light seeds at $16 \lesssim z \lesssim 18$ compared to the reference model (~ 4 times larger, on average), their BH masses are too small to activate efficient gas accretion, unless a much higher BH accretion efficiency (α_{BH}) or super-Eddington accretion is assumed (Volon-

teri & Rees 2005; Li 2012; Alexander & Natarajan 2014; Madau, Haardt & Dotti 2014; Pezzulli et al., in preparation).

4.2 Dependence on the critical dust-to-gas ratio

In the reference model, we assume that low-mass Pop II stars form when the metallicity of the star-forming gas reaches a critical value of $Z_{cr} = 10^{-3.8} \, Z_\odot$, above which metal fine-structure line cooling becomes efficient. However, semi-analytic and numerical studies suggest that gas cooling and fragmentation can be activated at a lower metallicity when dust grains are present (Schneider et al. 2002, 2006; Omukai, Hosokawa & Yoshida 2010; Dopcke et al. 2011). Schneider et al. (2012a) show that low-mass Pop II stars can form when the dust-to-gas mass ratio, $\mathcal{D}$, exceeds a critical value of $\mathcal{D}_{cr} = 4.4^{-1.9}_{-1.8} \times 10^{-9}$. Moreover, a dust-driven transition is consistent with observations of the tail of the metallicity distribution function of Galactic halo stars (Schneider et al. 2012b; de Bennassuti et al. 2014).

In GAMETE/QSODUST we follow dust enrichment in the ISM of all progenitor haloes and we can explore the effects of dust cooling and fragmentation on the formation of Pop III stars, hence of light BH seeds, and on the direct collapse of gas on to a heavy BH seed. Following Omukai et al. (2008), we assume that when $\mathcal{D} < \mathcal{D}_{cr}$ and $J_{LW} > J_{cr}$, the gas collapses almost isothermally until the densities are large enough to activate dust cooling and fragmentation, forming a compact Pop II stellar cluster. The middle panel of Fig. 9 shows that the effect is similar to imposing a larger LW flux critical threshold. A smaller number of light seeds are formed, heavy seed formation is suppressed and BH growth is dramatically inefficient, leading to $M_{BH} \sim 3 \times 10^4 \, M_\odot$ at $z = 6.4$. In fact, on average, dust enrichment allows most of the haloes to reach the critical threshold at $z \gtrsim 20$ (see the right-hand panel of Fig. 9), confining the formation of light seeds only in the first star-forming progenitors and preventing the formation of heavy seeds, as the condition $J_{LW} > J_{cr}$ is achieved only at smaller redshifts.

This conclusion does not depend on the fate of the newly formed dust-induced compact Pop II stellar clusters. Even assuming that their dynamical evolution favours the collapse into a BH of mass $\sim 10^3 \, M_\odot$ (Omukai et al. 2008; Devecchi & Volonteri 2009;
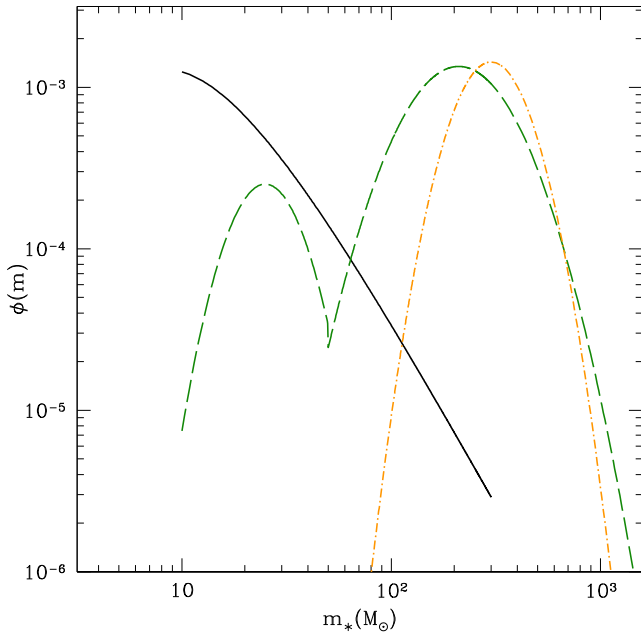
Figure 10. IMF of Pop III stars. The black solid line shows the Larson IMF adopted in the reference model, normalized to 1 in the mass range $[10-300]\,\mathrm{M_\odot}$. Green dashed and orange dot–dashed lines show the analytic functions used to approximate the results of Hirano et al. (2015) for $J_{\mathrm{LW}} < 0.1$ and >0.1, respectively. In both cases, the mass distribution is normalized to 1 in the mass range $[10-2000]\,\mathrm{M_\odot}$.

Devecchi et al. 2010, 2012), their number and mass are too small to significantly affect the BH mass growth rate.

4.3 IMF of Pop III stars

First attempts to predict the Pop III stellar mass spectrum ab initio, starting from cosmological initial conditions, have been recently made through sophisticated numerical simulations (Hirano et al. 2014, 2015). According to Hirano et al. (2015), Pop III stars which form in haloes exposed to an LW background intensity $J_{\mathrm{LW}} < 0.1$ follow a mass distribution characterized by two peaks, at ~ 25 and $\sim 250\,\mathrm{M_\odot}$. Conversely, only very massive ($>100\,\mathrm{M_\odot}$) stars form when $J_{\mathrm{LW}} > 0.1$ as less efficient cooling causes higher gas temperature and larger accretion rates (see fig. 6 in Hirano et al. 2015).

In order to test the implications of this environment-dependent Pop III IMF, we approximate the mass distribution found by Hirano et al. (2015) with the analytic functions shown in Fig. 10, where the IMF are normalized to 1 in the stellar mass range $[10-2000]\,\mathrm{M_\odot}$ (dashed and dot–dashed lines for $J_{\mathrm{LW}} < 0.1$ and >0.1, respectively). For comparison, we also show the IMF adopted in the reference model (solid line). Given the shape of the new distribution, we expect a larger number of massive Pop III remnants, leading to more frequent light BH seeds with mass $>300\,\mathrm{M_\odot}$ compared to the reference model.

The resulting average mass and redshift distributions of light seeds are shown in the left-hand and middle panels of Fig. 11. The two peaks of the mass distribution reflect the underlying Pop III IMF. The number of light BH seeds is ~ 10 times larger than in the reference model, and ~ 30 per cent of these have a mass $>300\,\mathrm{M_\odot}$. In fact, the shape of the underlying Pop III IMF affects the star formation history at $z > 15$ through both mechanical and chemical feedback: the larger number of stars with masses in the

pair-instability SN range, $160\,\mathrm{M_\odot} \lesssim m_* \lesssim 240\,\mathrm{M_\odot}$ (Heger & Woosley 2002), and above leads to strong SN- and AGN-driven outflows of metal-enriched gas out of the first mini-haloes. The integrated effect of this feedback-regulated SFR along the hierarchical evolution is to decrease the metallicity of gas-poor star-forming progenitors – favouring the formation of a larger number of Pop III BH remnants – and the LW emissivity, hence the intensity of the LW background. As a result, the condition $J_{\mathrm{LW}} > J_{\mathrm{cr}}$ is met at lower z compared to the reference model, when most of the Lyα haloes have already been enriched above the critical metallicity and the formation of heavy seeds is suppressed in 7 out of 10 merger trees.

In these conditions, the BH mass growth at $10 \lesssim z \lesssim 15$ is very sensitive to the amount of leftover gas from winds in progenitor systems. In the right-hand panel of Fig. 11, we show the BH mass growth and the contribution of light and heavy seeds as a function of redshift for four different merger tree simulations. In the top panels, we show the results for the same (b) and (g) merger tree realizations presented in Fig. 7. Despite no heavy seed is formed, $M_{\mathrm{BH}} \sim 10^9\,\mathrm{M_\odot}$ at $z \sim 6.4$ in simulation (b), only a factor of a few smaller than the observed value. Although the total BH mass contributed by light seeds is similar, gas accretion is less efficient in simulation (g) and the final BH mass is significantly smaller. In the bottom panel, we show the results of two simulations where, despite a comparable number of heavy seeds form, the final BH mass at $z \sim 6.4$ differs by almost two orders of magnitude. In simulation (f), a large number of light BH seeds form over the redshift range $17 \lesssim z \lesssim 25$. Gas depletion in their progenitor galaxies due to AGN feedback causes a lower average accretion rate at $z < 15$, and the BH mass at $z = 6.4$ is only $\sim 5 \times 10^7\,\mathrm{M_\odot}$. In contrast, the small number of light BH seeds formed in simulation (i) at $z \lesssim 20$ does not significantly affect the gas content of progenitor galaxies, and gas accretion at $z < 15$ can be efficient enough to form an SMBH at $z = 6.4$, with a mass consistent with the data.

4.4 Dynamics of light BH seeds

In the reference model, we assume that only the most massive Pop III remnant forms a light BH seed that settles at the galaxy centre accreting gas from the surrounding medium. To test the effect of this assumption, here we investigate the opposite, extreme scenario and we allow all BH remnants to merge and form a single more massive light BH seed that migrates at the centre of the galaxy. The underlying assumption is that the merging time-scale is shorter than the characteristic timestep of the simulation, and that dynamical effects, such as three-body scattering (Miller & Hamilton 2002; Gültekin, Miller & Hamilton 2006) and gravitational recoil (Haiman 2004; Shapiro 2005; Volonteri & Rees 2006), are not ejecting the merging BHs. Regarding three-body scattering, we can rescale the results by Gültekin, Miller & Hamilton (2004), Gültekin et al. (2006) and Miller & Lauburg (2009), while for the gravitational recoil we can use the Monte Carlo sampling of recoil velocities in Volonteri, Gültekin & Dotti (2010). In general, the potential well of the halo becomes sufficiently massive to retain merging and scattering BHs only when the halo mass is $\sim 10^7 - 10^8\,\mathrm{M_\odot}$. This is because most of the merging BHs have mass ratio between 1:6 and 1:1, where the recoil velocity is typically $>100\,\mathrm{km\,s^{-1}}$ for random spin magnitudes and configurations. Similarly, three-body scattering appears to cease to be effective in ejecting BHs when the escape velocity becomes $>100\,\mathrm{km\,s^{-1}}$. We note, however, that sudden gas inflows, triggered by mergers or collimated gas streams from the cosmic web, can temporarily deepen the potential well and allow mergers and three-body scattering to occur (Davies et al. 2011; Lupi
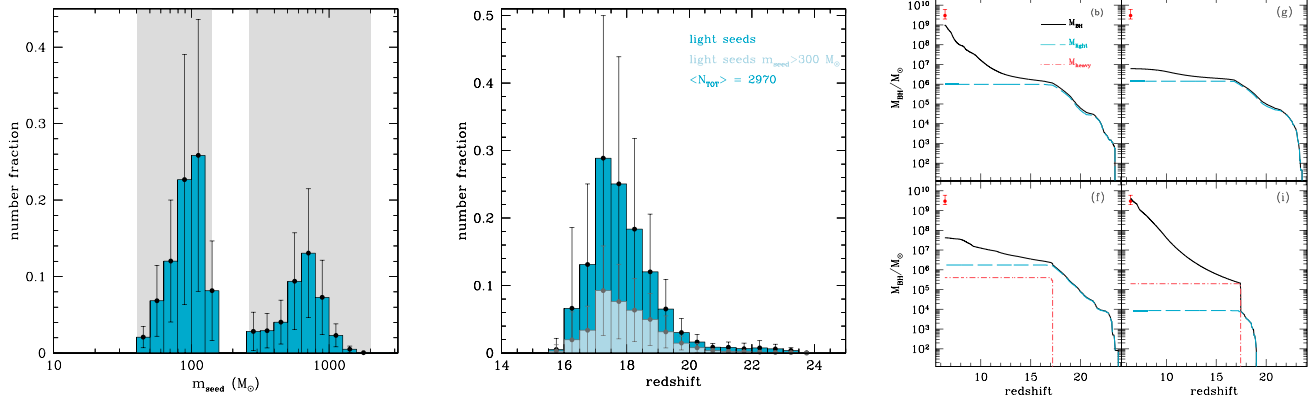
Figure 11. Same as Fig. 4 but only for light BH seeds and assuming the environment-dependent Pop III IMF predicted by Hirano et al. (2015). In the right-hand panel, we show the BH mass growth and the contribution of light and heavy seeds in four different realizations of the merger tree. The labels (b), (g), (f) and (i) are used to enable a direct comparison with the results presented in Fig. 7.

et al. 2014). We will in the following assume, optimistically, that all formed BHs can merge, but in reality we expect that only a fraction of them can be retained, and this fraction increases with the mass of the host halo.

The resulting mass and redshift distribution of light seeds is shown in the left-hand and middle panels of Fig. 12, respectively. As expected, the mass spectrum of light seeds now extends well beyond $300 \, M_\odot$, the maximum BH remnant mass for the adopted Pop III IMF. Less massive, more numerous, light seeds ($\lesssim 300 \, M_\odot$) form in less efficient star-forming haloes, while more massive light seeds ($> 300 \, M_\odot$) are the result of the coalescence of several (from few to hundreds) Pop III remnants formed in more efficient star-forming haloes. Interestingly, there is a tail of the mass distribution that extends up to $\sim 10^5 \, M_\odot$, showing that few light seeds may reach a mass comparable to that of heavy seeds.

The redshift distribution of light seeds is fairly independent of their mass, as shown by the two histograms in the middle panel of Fig. 12. Compared with the analogous plot for the reference model shown in Fig. 4, a much larger number of light seeds are formed. This is a consequence of the stronger feedback induced by more massive BHs on their host galaxy. In the shallow potential wells of small haloes at high redshift, BH feedback is able to unbind most – if not all – of the gas. As a result, the ISM metallicity remains below the critical value for a longer period of time, leading to a prolonged phase of Pop III star and light BH seed formation.

The effect on the BH mass growth rate is shown in the right-hand panel of Fig. 12. In this case, the contribution of light seeds exceeds that of heavy seeds, which is smaller (by a factor of ~ 3) than in the reference model, and triggers a faster and more efficient growth. The BH mass exceeds $\sim 10^9 \, M_\odot$ at $z \lesssim 10$ and reaches a final value of $\sim 6 \times 10^{10} \, M_\odot$ at $z \sim 6.4$, a factor of 20 larger than in the reference model.

5 CONCLUSIONS

We have investigated the origin of SMBHs at $z > 6$ applying a largely improved version of the semi-analytical model GA-METE/QSODUST. In this work, we explore the relative role of light BH seeds, formed as remnants of massive Pop III stars, and heavy BH seeds, formed by the direct collapse of gas, in the formation pathway to the first SMBHs.

To this aim, we have implemented a physically motivated pre-scription to estimate the cold gas mass fraction in mini-haloes, taking into account molecular and metal fine-structure cooling and the photodissociation of H_2 in the presence of an external LW back-ground. We then follow the subsequent evolution of the BHs and their host galaxies along the hierarchical history of a $z = 6.4$ halo with a mass of $10^{13} \, M_\odot$. The free parameters of the model, such as the accretion efficiency entering in the formulation of Eddington-limited Bondi accretion, the AGN wind efficiency, the efficiency of quiescent and merger-driven star formation, have been fixed to reproduce the observed properties of SDSS J1148. Simulating different merger trees of the same halo, we compute the intensity of the LW background, accounting for the contribution of stars and accreting BHs, the filling factor of ionized regions, the metal and dust enrichment in and outside the progenitor galaxies, to explore if and when heavy BH seeds can form in metal-poor Lyα haloes exposed to a strong LW background.

In the reference model, where we assume that Pop III stars form in progenitor galaxies with $Z < Z_{cr} = 10^{-3.8} \, Z_\odot$ according to a Larson IMF in the mass range $10 \, M_\odot \leq m_* \leq 300 \, M_\odot$, a small number of light BH seeds are hosted in mini-haloes at $z \gtrsim 20$ before radiative feedback is able to suppress H_2 cooling. The dominant fraction of light BH seeds form in Lyα cooling haloes at $15 \lesssim z \lesssim 20$, before the intensity of the LW background becomes larger than $J_{cr} = 300$ allowing the direct collapse of gas and the formation of heavy seeds. In these conditions, we find that in 9 out of 10 merger tree simulations between 3 and ~ 30 heavy seeds are able to form before metals have enriched all the progenitor galaxies to $Z \geq Z_{cr}$ and low-mass Pop II stars form. We find that the following.

(i) The growth of $z > 6$ SMBHs relies on heavy seeds. The only simulation where the interplay between chemical and radiative feedback effects prevents the formation of heavy seeds predicts a final BH mass of $M_{BH} < 10^6 \, M_\odot$.

(ii) The above result dramatically depends on the assumed values of J_{cr} and Z_{cr}. A larger value of J_{cr} ($= 10^3$) or a Pop III/Pop II transition driven by dust cooling at a critical dust-to-gas ratio of $\mathcal{D}_{cr} = 4.4 \times 10^{-9}$ prevents the formation of heavy seeds, hampering the mass growth of the nuclear BH so that its final mass at $z = 6.4$ is $M_{BH} < 10^6 \, M_\odot$ in all the merger tree simulations.

(iii) The relative importance of heavy and light BH seeds depends on the adopted IMF of Pop III stars, as this affects the history of
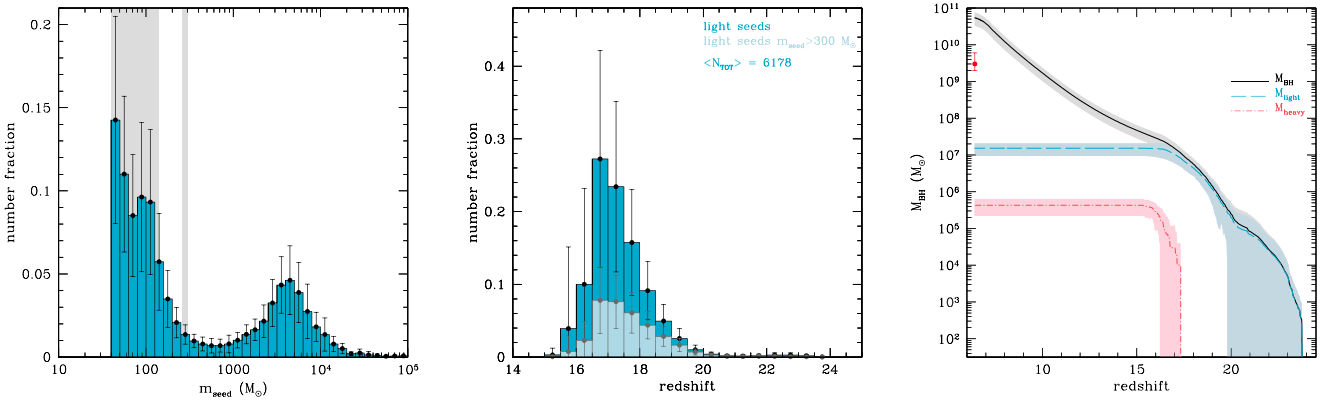
Figure 12. Same as in Figs 3 and 4 but assuming that all BH remnants of Pop III stars merge to form a single more massive BH seed. In addition, in the middle panel we show the redshift distribution of light seeds with masses >300 M$_\odot$ (azure histogram and grey data points).

cold gas along the merger tree by means of SN- and AGN-driven winds.

(iv) As long as gas accretion is assumed to be Eddington-limited, the mass of individual BH seeds is the key condition to trigger SMBH growth. If all BH remnants merge before settling to the centre of their progenitor galaxy, the mass distribution of light BH seeds extends to $\sim 10^3 - 10^5$ M$_\odot$. In these conditions, gas accretion is so efficient that by $z = 6.4$ the SMBH mass is – on average – $>10^{10}$ M$_\odot$ and the evolution is completely dominated by light BH seeds.

We conclude that the formation of a $>10^9$ M$_\odot$ BH at $z > 6$ depends on a complex interplay of feedback processes, where the mass and redshift distributions of both light and heavy seeds have a fundamental role. The first SMBHs can grow by Eddington-limited accretion only if sufficiently massive BH seeds are able to form in their progenitor galaxies. This can be achieved by means of Pop III BH remnants (light seeds) if Pop III stars form with $m_* > 300$ M$_\odot$ or if smaller mass BH remnants merge to form a single, more massive BH. Alternatively, even a few heavy seeds with mass $\sim 10^5$ M$_\odot$ can provide the right 'head start', but their formation requires favourable conditions that can only be achieved if $J_{cr} \lesssim 300$ and $Z_{cr} \geq 10^{-3.8}$ Z$_\odot$. Since $J_{cr} < 300$ is lower than required by 3D cosmological simulations of the collapse of primordial clouds, alternative models of direct collapse driven by dynamical processes should be kept in mind (e.g. Loeb & Rasio 1994; Eisenstein & Loeb 1995; Begelman et al. 2006; Mayer et al. 2007; Volonteri & Begelman 2010).

In our reference model, where the formation of an SMBH relies on heavy seeds, the number of heavy seed progenitors varies between 3 and 27 among the different merger tree simulations, with an average number of 13. If we weight these numbers by the observed comoving density of quasars at $z = 6$, $n_{SMBH} \sim 10^{-9}$ cMpc^{-3}, we can predict the comoving number density of DCBHs. This is shown in Fig. 13, where we compare the results of our reference model with other studies. We find that by $z \sim 15$ the comoving number density of DCBH is 3×10^{-9} cMpc$^{-3} \lesssim n_{DCBH} \lesssim 2.7 \times 10^{-8}$ cMpc^{-3}. We clarify that these numbers refer to heavy BH seed progenitors of SMBHs at $z = 6$. In the same reference model, a much larger population of DCBHs form (~ 100 on average) which – however – end up as satellites and do not directly contribute to the mass growth of the SMBH. For these enlarged population, the comoving number
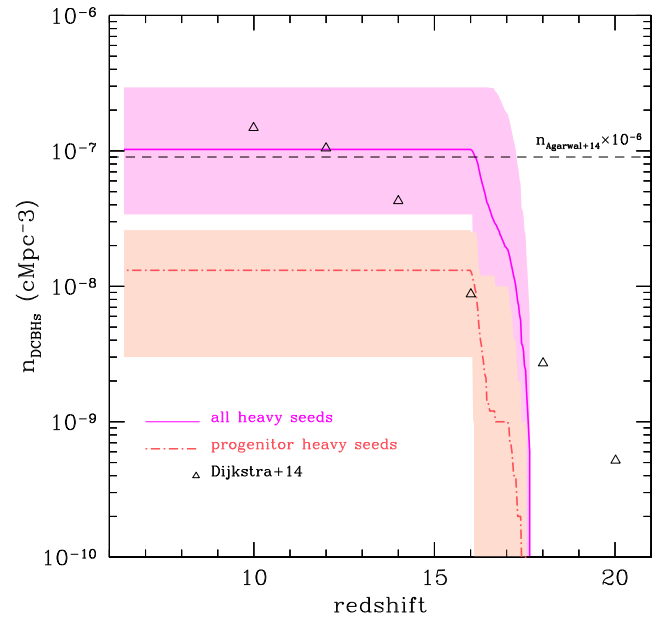

Figure 13. Predicted number density of DCBHs as a function of z. The solid line shows the average number of all DCBHs formed in the reference model and the dot–dashed line shows the same quantity for real DCBH progenitors (see the text). For each of these two classes, the shades span the values found in different merger tree simulations. For comparison, we also show the values predicted by Dijkstra et al. (2014, triangles) and Agarwal et al. (2014, horizontal dashed line). The latter value has been multiplied by 10^{-6} to enable the comparison.

density that we predict is $\sim 10^{-7}$ cMpc^{-3}, in very good agreement with the results of Dijkstra et al. (2014) for their fiducial model. A much larger value has been found by Agarwal et al. (2014), who report ~ 6 potential DCBH hosts in their 4 cMpc size simulation box at $z \sim 10$, leading to an estimated comoving number density of ~ 0.09 cMpc^{-3}. As already noted by Dijkstra et al. (2014), the main reason for this discrepancy is that Agarwal et al. (2014) adopt $J_{cr} = 30$. No DCBH would form in their box if $J_{cr} = 300$ were to be assumed (see the bottom panel of their fig. 1).

Compared to these previous analyses, our study allows us to identify BH seeds that are the progenitors of the first SMBHs, and to study the conditions that allow these BH seeds to germinate.

ACKNOWLEDGEMENTS

REFERENCES

Abel T., Bryan G. L., Norman M. L., 2002, Science, 295, 93

Agarwal B., Khochfar S., Johnson J. L., Neistein E., Dalla Vecchia C., Livio M., 2012, MNRAS, 425, 2854

Agarwal B., Dalla Vecchia C., Johnson J. L., Khochfar S., Paardekooper J.-P., 2014, MNRAS, 443, 648

Agarwal B., Smith B., Glover S., Natarajan P., Khochfar S., 2015, preprint (arXiv:1504.04042)

Ahn K., Shapiro P. R., Iliev I. T., Mellema G., Pen U.-L., 2009, ApJ, 695, 1430

Alexander T., Natarajan P., 2014, Science, 345, 1330

Anders E., Grevesse N., 1989, Geochim. Cosmochim. Acta, 53, 197

Barkana R., Loeb A., 1999, ApJ, 523, 54

Barth A. J., Martini P., Nelson C. H., Ho L. C., 2003, ApJ, 594, L95

Begelman M. C., Volonteri M., Rees M. J., 2006, MNRAS, 370, 289

Bromm V., 2013, Rep. Prog. Phys., 76, 112901

Bromm V., Loeb A., 2003, ApJ, 596, 34

Bromm V., Ferrara A., Coppi P. S., Larson R. B., 2001, MNRAS, 328, 969

Bruzual G., Charlot S., 2003, MNRAS, 344, 1000

Ciardi B., Ferrara A., Abel T., 2000, ApJ, 533, 594

Cicone C. et al., 2015, A&A, 574, A14

Davies M. B., Miller M. C., Bellovary J. M., 2011, ApJ, 740, L42

de Bennassuti M., Schneider R., Valiante R., Salvadori S., 2014, MNRAS, 445, 3039

De Rosa G., Decarli R., Walter F., Fan X., Jiang L., Kurk J., Pasquali A., Rix H. W., 2011, ApJ, 739, 56

De Rosa G. et al., 2014, ApJ, 790, 145

Devecchi B., Volonteri M., 2009, ApJ, 694, 302

Devecchi B., Volonteri M., Colpi M., Haardt F., 2010, MNRAS, 409, 1057

Devecchi B., Volonteri M., Rossi E. M., Colpi M., Portegies Zwart S., 2012, MNRAS, 421, 1465

Di Matteo T., Springel V., Hernquist L., 2005, Nature, 433, 604

Dijkstra M., Haiman Z., Mesinger A., Wyithe J. S. B., 2008, MNRAS, 391, 1961

Dijkstra M., Ferrara A., Mesinger A., 2014, MNRAS, 442, 2036

Dopcke G., Glover S. C. O., Clark P. C., Klessen R. S., 2011, ApJ, 729, L3

Eisenstein D. J., Loeb A., 1995, ApJ, 443, 11

Fan X. et al., 2001, AJ, 122, 2833

Fan X. et al., 2004, AJ, 128, 515

Ferrara A., Salvadori S., Yue B., Schleicher D., 2014, MNRAS, 443, 2410

Glover S., 2013, in Wiklind T., Mobasher B., Bromm V., eds, Astrophysics and Space Science Library, Vol. 396, The First Galaxies. Springer-Verlag, Berlin, p. 103

Glover S. C. O., 2015a, MNRAS, 451, 2082

Glover S. C. O., 2015b, MNRAS, 453, 2901

Gültekin K., Miller M. C., Hamilton D. P., 2004, ApJ, 616, 221

Gültekin K., Miller M. C., Hamilton D. P., 2006, ApJ, 640, 156

Haardt F., Madau P., 1996, ApJ, 461, 20

Haiman Z., 2004, ApJ, 613, 36

Haiman Z., Loeb A., 1997, ApJ, 483, 21

Haiman Z., Thoul A. A., Loeb A., 1996, ApJ, 464, 523

Haiman Z., Rees M. J., Loeb A., 1997, ApJ, 476, 458

Haiman Z., Abel T., Rees M. J., 2000, ApJ, 534, 11

Hartwig T., Glover S. C. O., Klessen R. S., Latif M. A., Volonteri M., 2015, MNRAS, 452, 1233

Heger A., Woosley S. E., 2002, ApJ, 567, 532

Heger A., Fryer C. L., Woosley S. E., Langer N., Hartmann D. H., 2003, ApJ, 591, 288

Hirano S., Hosokawa T., Yoshida N., Umeda H., Omukai K., Chiaki G., Yorke H. W., 2014, ApJ, 781, 60

Hirano S., Hosokawa T., Yoshida N., Omukai K., Yorke H. W., 2015, MNRAS, 448, 568

Hosokawa T., Omukai K., Yoshida N., Yorke H. W., 2011, Science, 334, 1250

Hosokawa T., Omukai K., Yorke H. W., 2012, ApJ, 756, 93

Hosokawa T., Yorke H. W., Inayoshi K., Omukai K., Yoshida N., 2013, ApJ, 778, 178

Inayoshi K., Haiman Z., 2014, MNRAS, 445, 1549

Inayoshi K., Omukai K., 2011, MNRAS, 416, 2748

Inayoshi K., Omukai K., 2012, MNRAS, 422, 2539

Inayoshi K., Tanaka T. L., 2015, MNRAS, 450, 4350

Inayoshi K., Omukai K., Tasker E., 2014, MNRAS, 445, L109

Johnson J. L., Whalen D. J., Fryer C. L., Li H., 2012, ApJ, 750, 66

Johnson J. L., Whalen D. J., Li H., Holz D. E., 2013, ApJ, 771, 116

Johnson J. L., Whalen D. J., Agarwal B., Paardekooper J.-P., Khochfar S., 2014, MNRAS, 445, 686

Katz H., Sijacki D., Haehnelt M. G., 2015, MNRAS, 451, 2352

Larson R. B., 1998, MNRAS, 301, 569

Latif M. A., Volonteri M., 2015, MNRAS, 452, 1026

Latif M. A., Schleicher D. R. G., Schmidt W., Niemeyer J., 2013a, MNRAS, 433, 1607

Latif M. A., Schleicher D. R. G., Schmidt W., Niemeyer J. C., 2013b, MNRAS, 436, 2989

Latif M. A., Bovino S., Van Borm C., Grassi T., Schleicher D. R. G., Spaans M., 2014a, MNRAS, 443, 1979

Latif M. A., Schleicher D. R. G., Bovino S., Grassi T., Spaans M., 2014b, ApJ, 792, 78

Li L.-X., 2012, MNRAS, 424, 1461

Loeb A., Rasio F. A., 1994, ApJ, 432, 52

Lupi A., Colpi M., Devecchi B., Galanti G., Volonteri M., 2014, MNRAS, 442, 3616

Machacek M. E., Bryan G. L., Abel T., 2001, ApJ, 548, 509

Madau P., Rees M. J., 2001, ApJ, 551, L27

Madau P., Ferrara A., Rees M. J., 2001, ApJ, 555, 92

Madau P., Haardt F., Dotti M., 2014, ApJ, 784, L38

Maiolino R. et al., 2012, MNRAS, 425, L66

Mayer L., Kazantzidis S., Madau P., Colpi M., Quinn T., Wadsley J., 2007, Science, 316, 1874

Miller M. C., Hamilton D. P., 2002, MNRAS, 330, 232

Miller M. C., Lauburg V. M., 2009, ApJ, 692, 917

Mortlock D. J. et al., 2011, Nature, 474, 616

Oh S. P., Haiman Z., 2002, ApJ, 569, 558

Omukai K., 2001, ApJ, 546, 635

Omukai K., 2012, PASJ, 64, 114

Omukai K., Nishi R., 1999, ApJ, 518, 64

Omukai K., Tsuribe T., Schneider R., Ferrara A., 2005, ApJ, 626, 627

Omukai K., Schneider R., Haiman Z., 2008, ApJ, 686, 801

Omukai K., Hosokawa T., Yoshida N., 2010, ApJ, 722, 1793

Petri A., Ferrara A., Salvaterra R., 2012, MNRAS, 422, 1690

Pollack J. B., Hollenbach D., Beckwith S., Simonelli D. P., Roush T., Fong W., 1994, ApJ, 421, 615

Rees M. J., 1978, The Observatory, 98, 210

Regan J. A., Johansson P. H., Wise J. H., 2014, ApJ, 795, 137

Ricotti M., Gnedin N. Y., Shull J. M., 2001, ApJ, 560, 580

Salvadori S., Ferrara A., 2009, MNRAS, 395, L6

Salvadori S., Ferrara A., 2012, MNRAS, 421

Salvadori S., Schneider R., Ferrara A., 2007, MNRAS, 381, 647

Salvadori S., Ferrara A., Schneider R., 2008, MNRAS, 386, 348

Salvadori S., Tolstoy E., Ferrara A., Zaroubi S., 2014, MNRAS, 437, L26

Salvadori S., Skúladóttir Á., Tolstoy E., 2015, MNRAS, 454, 1320

Sazonov S. Y., Ostriker J. P., Sunyaev R. A., 2004, MNRAS, 347, 144

Schaerer D., 2002, A&A, 382, 28

Schneider R., Ferrara A., Natarajan P., Omukai K., 2002, ApJ, 571, 30

Schneider R., Ferrara A., Salvaterra R., Omukai K., Bromm V., 2003, Nature, 422, 869

Schneider R., Omukai K., Inoue A. K., Ferrara A., 2006, MNRAS, 369, 1437

Schneider R., Omukai K., Bianchi S., Valiante R., 2012a, MNRAS, 419, 1566

Schneider R., Omukai K., Limongi M., Ferrara A., Salvaterra R., Chieffi A., Bianchi S., 2012b, MNRAS, 423, L60

Shakura N. I., Sunyaev R. A., 1973, A&A, 24, 337

Shang C., Bryan G. L., Haiman Z., 2010, MNRAS, 402, 1249

Shapiro S. L., 2005, ApJ, 620, 59

Shapiro P. R., Iliev I. T., Raga A. C., 2004, MNRAS, 348, 753

Sobacchi E., Mesinger A., 2013, MNRAS, 432, 3340

Spaans M., Silk J., 2006, ApJ, 652, 902

Sugimura K., Omukai K., Inoue A. K., 2014, MNRAS, 445, 544

Sugimura K., Coppola C. M., Omukai K., Galli D., Palla F., 2016, MNRAS, 456, 270

Susa H., Hasegawa K., Tominaga N., 2014, ApJ, 792, 32

Sutherland R. S., Dopita M. A., 1993, ApJS, 88, 253

Tanaka T., Haiman Z., 2009, ApJ, 696, 1798

Tutukov A. V., Shustov B. M., Wiebe D. S., 2000, Astron. Rep., 44, 711

Valiante R., Schneider R., Salvadori S., Bianchi S., 2011, MNRAS, 416, 1916

Valiante R., Schneider R., Maiolino R., Salvadori S., Bianchi S., 2012, MNRAS, 427, L60

Valiante R., Schneider R., Salvadori S., Gallerani S., 2014, MNRAS, 444, 2442

Volonteri M., 2010, ARA&A, 18, 279

Volonteri M., Begelman M. C., 2010, MNRAS, 409, 1022

Volonteri M., Bellovary J., 2012, Rep. Prog. Phys., 75, 124901

Volonteri M., Rees M. J., 2005, ApJ, 633, 624

Volonteri M., Rees M. J., 2006, ApJ, 650, 669

Volonteri M., Gültekin K., Dotti M., 2010, MNRAS, 404, 2143

Volonteri M., Silk J., Dubus G., 2015, ApJ, 804, 148

Willott C. J., McLure R. J., Jarvis M. J., 2003, ApJ, 587, L15

Wolcott-Green J., Haiman Z., Bryan G. L., 2011, MNRAS, 418, 838

Wolfire M. G., Hollenbach D., McKee C. F., Tielens A. G. G. M., Bakes E. L. O., 1995, ApJ, 443, 152

Wu X.-B. et al., 2015, Nature, 518, 512

Yoshida N., Omukai K., Hernquist L., 2008, Science, 321, 669

Yue B., Ferrara A., Salvaterra R., Xu Y., Chen X., 2014, MNRAS, 440, 1263

APPENDIX A: HALO GAS COOLING EFFICIENCY

In each DM halo, the fraction of gas mass that is able to cool is set by the balance between the cooling time and the dynamical time. Here we adopt a procedure similar to that presented in Madau, Ferrara & Rees (2001).

We compute the free-fall time as

$$t_{\mathrm{ff}}(r) = \int_0^r \frac{\mathrm{d}r'}{\sqrt{v_\mathrm{e}^2(r') - v_\mathrm{e}^2(r)}} \left(= \int_0^r \frac{\mathrm{d}r'}{v_r(r')} \right), \tag{A1}$$

where v_e is the escape velocity (v_r is the infall velocity of a test particle at rest at r), DM haloes are assumed to have a Navarro, Frenk & White (NFW) density profile with concentration parameter $c = 4.8$, and the gas follows an isothermal gas density distribution (see equations 9, 18 and 21 in Madau et al. 2001).

The cooling time is defined as

$$t_{\mathrm{cool}}(r) = \frac{3\, n\, k\, T_{\mathrm{vir}}}{2\, \Lambda(n, Z)}, \tag{A2}$$

where k is Boltzmann's constant, n is the gas number density and $\Lambda(n, Z)$ is the density and metallicity-dependent cooling rate per unit volume.

The parameter f_{cool} introduced in Section 2.3 is defined as the ratio between the gas mass within a radius r_{cool} such that $t_{\mathrm{cool}}(r_{\mathrm{cool}}) = t_{\mathrm{ff}}(r_{\mathrm{cool}})$ and the total gas mass within the virial radius.

In Lyα haloes, even in primordial conditions the gas can efficiently cool by means of H and He transitions. Hence, we assume that in these systems $f_{\mathrm{cool}} = 1$ and the SFR is only limited by the infall rate (see equation 7).[6]

In mini-haloes the cooling time can be longer than the free-fall time at most radii, so that $f_{\mathrm{cool}} \ll 1$. The exact value of this parameter depends on the virial temperature, redshift (hence halo mass) and metallicity of the gas. The cooling rate is computed considering a simplified version of the chemical evolution model of Omukai (2012) that we describe below.

Cooling and heating processes. To compute the cooling rate, we consider the following physical processes: H Lyα emission ($\Lambda_{\mathrm{Ly}\alpha}$), H_2 rovibrational emission (Λ_{H_2}), and C II and O I fine-structure line emission ($\Lambda_{\mathrm{C\,II}}$, $\Lambda_{\mathrm{O\,I}}$). Photoelectric emission by dust (Γ_{PE}) is also taken on to account as it provides an important heating process when the medium is dust-enriched and in the presence of a far-UV (FUV) background (Wolfire et al. 1995). For simplicity, we assume the same spectral shape in the Galactic ISM and we take the Habing parameter for the FUV to be $G_0 = 2.9 \times 10^{-2} J_{\mathrm{LW}}$. Hence, the total cooling rate is computed as

$$\Lambda = \Lambda_{\mathrm{Ly}\alpha} + \Lambda_{H_2} + \Lambda_{\mathrm{C\,II}} + \Lambda_{\mathrm{O\,I}} - \Gamma_{\mathrm{PE}}. \tag{A3}$$

Ionization degree. The post-recombination leftover electron fraction is $y_{\mathrm{e,prim}} \sim 2 \times 10^{-4}$. Following virialization, the ionization degree can increase due to collisional ionization:

$$\mathrm{H} + \mathrm{e} \rightarrow \mathrm{H}^+ + 2\mathrm{e} \tag{A4}$$

followed by radiative recombination:

$$\mathrm{H}^+ + \mathrm{e} \rightarrow \mathrm{H} + \gamma. \tag{A5}$$

Hence, the ionization fraction reaches an equilibrium value given by

$$y_{\mathrm{e,eq}} = \frac{k_{\mathrm{ion}}}{k_{\mathrm{ion}} + k_{\mathrm{rec}}}. \tag{A6}$$

In the model, we take the ionization degree to be $y_\mathrm{e} = \max(y_{\mathrm{e,prim}}; y_{\mathrm{e,eq}})$ and the atomic hydrogen fraction as $y_\mathrm{H} \sim 1 - y_\mathrm{e}$ because the molecular fraction is always $\ll 1$.

Molecular fraction. Molecular hydrogen can form from the gas phase via the H^- channel:

$$\mathrm{H} + \mathrm{e} \rightarrow \mathrm{H}^- + \gamma \tag{A7}$$

$$\mathrm{H}^- + \mathrm{H} \rightarrow H_2 + \mathrm{e} \tag{A8}$$

or on the surface of dust grains. In one free-fall time, the H_2 fraction formed can be approximated as

$$y_{H_2,\mathrm{form}} = \frac{k_{\mathrm{H}^-,\mathrm{form}}}{k_{\mathrm{rec}}} \ln\left(1 + \frac{t_{\mathrm{ff}}}{t_{\mathrm{rec}}}\right) + k_{\mathrm{dust,form}}\, y_\mathrm{H}\, n\, t_{\mathrm{ff}}, \tag{A9}$$

---

[6] This condition is strictly true only at $z \geq 9$ for haloes with $T_{\mathrm{vir}} < 5 \times 10^5$ K. In fact, above this temperature and in primordial conditions the cooling rate is dominated by free–free emission. Here we assume $f_{\mathrm{cool}} = 1$ for all Lyα haloes because most of these larger virial temperatures (mass) haloes are already metal-enriched when they first appear along the merger tree and therefore the cooling rate is dominated by highly ionized metal species (Sutherland & Dopita 1993).
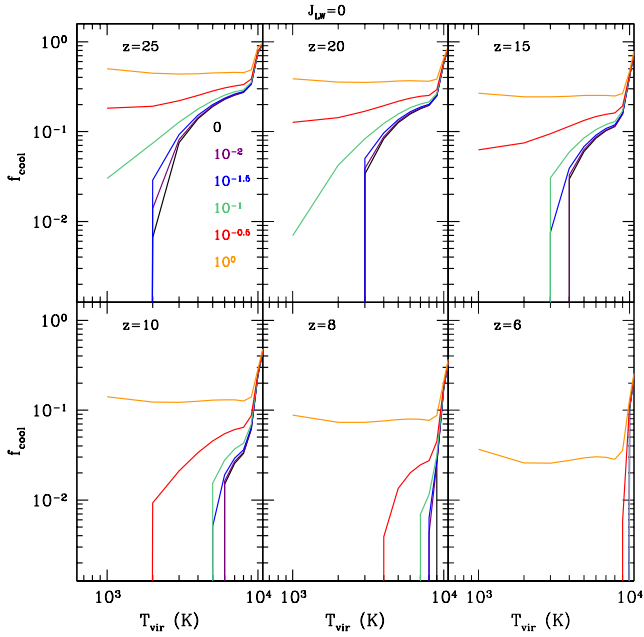
Figure A1. The mass fraction of gas that is able to cool in one free-fall time, f_{cool}, as a function of halo virial temperature for $J_{LW} = 0$. Each line represents a fixed gas metallicity: $Z = 0$ (black), 10^{-2} (violet), $10^{-1.5}$ (blue), 10^{-1} (green), $10^{-0.5}$ (red), 1 (yellow), in solar units. Here we consider the presence of dust grains (see the text). Different panels are for different redshift, from $z = 25$ to 6, as labelled in the figure.
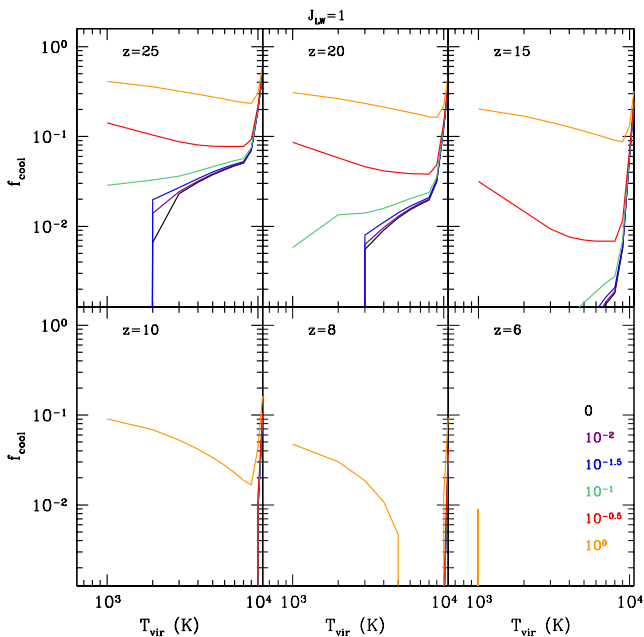

Figure A2. Same as Fig. A1 but for $J_{LW} = 1$.

Figure A3. Same as Fig. A1 but for $J_{LW} = 10$.
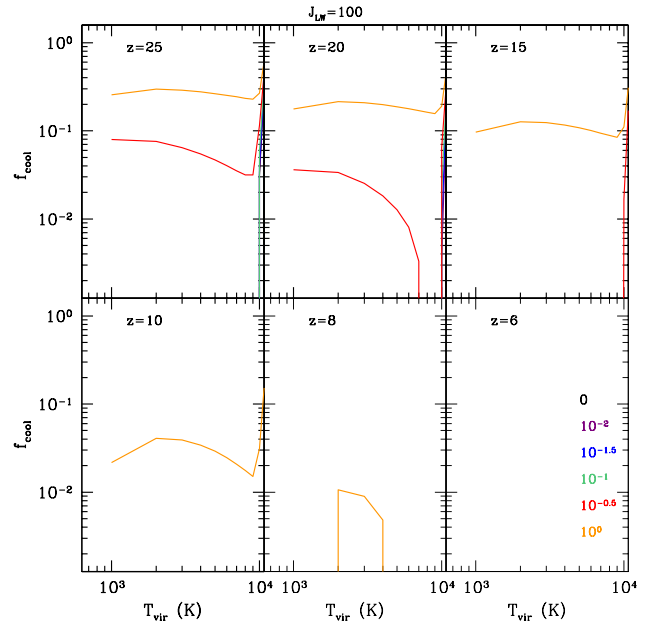
Figure A4. Same as Fig. A1 but for $J_{LW} = 100$.

where $k_{H^-,form} n_H n_e$ is the H$_2$ formation rate via the H$^-$ channel, $k_{dust, form}$ is the H$_2$ formation rate on dust grains and the recombination time is

$$t_{rec} = \frac{1}{k_{rec} \, y_e \, n}. \qquad (A10)$$

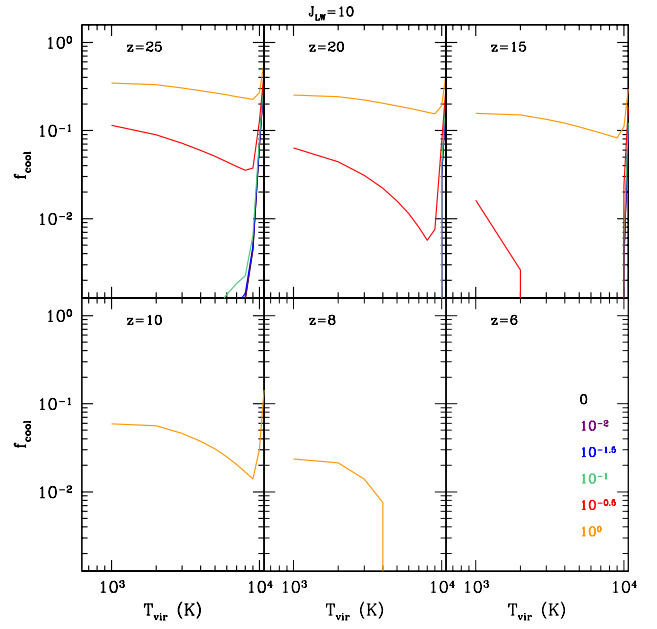In the presence of an LW background, the H$_2$ fraction reaches an equilibrium value given by (Anders & Grevesse 1989)

$$y_{H_2,eq} = \left(k_{H^-,form} \, y_e + k_{dust,form} \right) \frac{y_H \, n}{k_{dis}}, \qquad (A11)$$

where k_{dis} is the H$_2$ dissociation coefficient and it is calculated considering the H$_2$ self-shielding factor as in Wolcott-Green, Haiman & Bryan (2011). In the model, we take the H$_2$ fraction to be $y_{H_2} = \min(y_{H_2,form}; y_{H_2,eq})$.

Metal fractions For simplicity, at each given metallicity Z all the carbon atoms are assumed to be in C II and the oxygen atoms in O I, with an elemental abundance given by

$$y_{C\,II} = 3.97 \times 10^{-4} \frac{Z}{Z_\odot} \qquad y_{O\,I} = 8.49 \times 10^{-4} \frac{Z}{Z_\odot}. \qquad (A12)$$

When dust grains are present, we account for partial depletion of these two elements on dust grains and we assume an elemental fraction of (Pollack et al. 1994)

$$y_{C\,II} = 0.93 \times 10^{-4} \frac{Z}{Z_\odot} \qquad y_{O\,I} = 3.57 \times 10^{-4} \frac{Z}{Z_\odot}. \qquad (A13)$$

Using the above prescription, we run a large set of models, changing the virial temperature, redshift, gas metallicity, and the value of the external LW background, and we compute the corresponding f_{cool}. The results are summarized in Figs A1–A4. When $Z = 0$, f_{cool} is a strong function of T_{vir}. In the absence of an LW background (see Fig. A1), f_{cool} drops from ~ 1 to ~ 0.1 in the temperature range $8000\,\mathrm{K} \leq T_{vir} < 10^4\,\mathrm{K}$, followed by a smoother decline to $\sim 10^{-2}$ at $T_{vir} \sim 10^3\,\mathrm{K}$. Even in these favourable conditions (no H_2 dissociation), for a fixed T_{vir}, f_{cool} strongly depends on redshift. This reflects the density dependence of the cooling rate, which – for the same physical conditions – leads to a shorter cooling time at high redshift. This result holds even when the gas metallicity is $Z > 0$. Significant deviations from the primordial case require a metallicity of $Z \geq 0.1\,Z_\odot$ at $z \gtrsim 20$, of $Z \geq 0.5\,Z_\odot$ at $10 \lesssim z \lesssim 15$ and of $Z \geq Z_\odot$ at $6 \lesssim z \lesssim 8$. Finally, at $z < 6$ we find that – independently of the gas metallicity – gas cooling in mini-haloes is suppressed.

Figs A2–A4 show how the above results change when the intensity of the LW background ranges within $1 \leq J_{LW} \leq 10^2$. As expected, the largest effect is in the behaviour of the $Z < 0.1\,Z_\odot$ gas, which can cool only if $J_{LW} \lesssim 1$ and $z \gtrsim 20$.

This paper has been typeset from a TEX/LATEX file prepared by the author.